Available online at www.sciencedirect.com
SCIENCE DIRECT®
ELSEVIER
Tectonophysics 365 (2003) 103–127
TECTONOPHYSICS
www.elsevier.com/locate/tecto

The structure and the phyllosilicates (chemistry, crystallinity and texture) of Talas Ala-Tau (Tien Shan, Kyrgyz Republic): comparison with more recent subduction complexes

Isabel Abad[a], Gabriel Gutiérrez-Alonso[b,*], Fernando Nieto[a], Igor Gertner[c], Alex Becker[d], Ana Cabero[b]

[a] *Instituto Andaluz de Ciencias de la Tierra y Departamento de Mineralogía y Petrología, Universidad de Granada. 18002, Granada, Spain*
[b] *Departamento de Geología, Universidad de Salamanca. 37008, Salamanca, Spain*
[c] *Geology and Geography Department, Tomsk State University, Lenin Street 36, Tomsk 634050, Russia*
[d] *Tectonic Consulting LDT, 1061 Brickley Close, North Saanich, Canada V8L 5L1*

Received 30 January 2002; accepted 23 September 2002

Abstract

Geological mapping and structural analysis of the Talas Ala Tau (Tien Shan, Kyrgyz Republic) have revealed a complex structure composed of folds with axial-plane cleavage and thrust faults verging towards the NE. The main structures of the range correspond to minor Tertiary and Carboniferous–Permian deformation superimposed on the main deformation event that took place during the Baikalian orogeny. The pervasive axial-plane cleavage diminishes in penetrativity from the hinterland to the foreland in both the Uzunakhmat and Karagoin sheets. The main thrusts developed phyllonitic shear-related rocks on the hangingwall immediately above the thrust planes. A crystal-chemical study of the phyllosilicates growth during the Baikalian deformation event along a cross-section revealed changes in the crystallinity, composition and lattice parameters of them. The phyllosilicates present in the Talas Ala Tau rocks were crystallized in very low-grade metamorphic conditions, that is below 300 °C, as indicated by their Kübler Index (KI), which decreases from SW towards the NE. Detailed TEM study of the phyllosilicates reveals a clear textural difference at the lattice level between samples with higher or lower KI parameters. There is also a clear difference in crystal-chemical parameters (KI and *b*) and composition between the phyllosilicates growth in relation to the axial-plane cleavage and the ones belonging to the thrust-related phyllonites. The first ones are more affected by the ferrimuscovitic vector than the phyllosilicates of phyllonites, closer to the theoretical phengitic component. Huge ranges of values of phengitic content of micas at sample level are interpreted as the result of a decompression path from at least 8 kbar. We propose a subduction geodynamic environment for the regional deformation and the origin of the phyllosilicates, as they are similar to those obtained in more recent accretionary complexes.
© 2003 Elsevier Science B.V. All rights reserved.

Keywords: Tien Shan; Structure; Baikalian; White mica; Crystallinity; HRTEM; Subduction complex

* Corresponding author.
E-mail address: gabi@usal.es (G. Gutiérrez-Alonso).

0040-1951/03/$ - see front matter © 2003 Elsevier Science B.V. All rights reserved.
doi:10.1016/S0040-1951(03)00018-0

1. Introduction

Micas are minerals that provide large amounts of information regarding very low and low-grade metamorphic processes, and therefore useful in deciphering the processes involved from diagenesis to regional deformation. Because of the sensitivity of the crystal-chemical parameters of micas to temperature, pressure and deformation (finite strain) changes, they can be traced along complex, multiphase deformation events (Frey et al., 1980; Johnson and Oliver, 1990; Gutiérrez-Alonso and Nieto, 1996; etc.).

Merriman and Frey (1999) reviewed the regional patterns of very low-grade metamorphism and concluded that extensional, accretionary and collisional settings can be distinguished only by a combination of structural, sedimentological and mineralogical criteria (see Table 3.1 of Merriman and Frey, 1999). The prograde sequence of metapelitic zones developed by very low-grade metamorphism is the result of reaction progress in clay minerals promoted by the interaction of basin heat flow and strain associated with overburden and tectonic stresses.

The Talas Ala Tau area provides an excellent place for combining field geology and structural analysis with phyllosilicate mineralogical techniques along a complete composite cross-section, more than 15 km long, with outstanding outcrops. The different structures, developed under very low to low-grade metamorphic conditions, have been deformed representing a variety of different mechanisms ranging from layer-parallel shortening, to folding and mechanical grain size reduction and recrystallization (cataclasis and mylonitization), leading to the generation of cleavages with different grades of penetrativity and the recrystallization of micas with different characteristics.

The Talas Ala Tau is a good region to test the validity and application of micas to trace deformation and metamorphic changes as well as to help to interpret a part of its geologic history that has not been described before. The use of multiple techniques to characterize the composition, textural relationships and crystal-chemical properties of the micas has resulted in a large dataset able to trace and determine the changes in the different characteristics of the phyllosilicates, and to relate them to the varying conditions of rock deformation experienced throughout this area. A comparison is made with modern subduction-related analogues in an attempt to compare recent and ancient deformation events in similar scenarios.

2. Geological setting

Because of the Cenozoic collision between India and Eurasia, several intracratonic belts were reactivated, giving rise to mountain belts across Central Asia. In addition to the Himalaya, the most important one are the Tien Shan Ranges which reaches more than 7000 m in height. The uplift and subsequent erosion of these mountains has allowed the exposure of rocks belonging to previous orogenic events that were responsible of the building and amalgamation of the Asian continent (Abdrakhmatov et al., 1996; Bullen et al., 2001). The main orogenic process involved in the Tien Shan Cordillera was the Upper Paleozoic Uralian–Mongolian (equivalent to Variscan–Hercynian), which followed a long-lived subduction, and that resumed the closing of the paleo-Turkestan Ocean as a result of the collision of the Kipchack arc and the Karakum–Tarim continent (Sengör et al., 1993; Sengör and Natal'in, 1996). The geologic framework of NW Tien Shan, which partly crops out in the Kyrgyz Republic, can be divided into three main domains (Fig. 1): The South and Middle Tien Shan Domains, characterized by the only occurrence of the aforementioned Uralian–Variscan deformation and the Northern Tien Shan, characterized by the presence of pre-Uralian deformation events of Baikalian–Cadomian age (from middle Riphean until Late Proterozoic–Cambro-Ordovician?, Kiselev et al., 1988; Allen et al., 2001) that imparted widespread axial-plane cleavage and was responsible for the origin of most of the thrusts present in the area.

Within the North Tien Shan, the Talas Ala Tau is one of the most important outcrops of Precambrian rocks in the region. The Precambrian rocks, mostly Riphean sedimentary rocks (Korolev and Maksumova, 1980; Kiselev and Korolev, 1981), crop out in two thrust-limited domains named the Uzunakhmat (to the SW) and the Karagoin (to the NE) sheets (Fig. 2). The thrust that separates both domains is known as the Kumyshtak thrust and its displacement, although unknown because the lack of suitable markers, is interpreted to be more than 10 km.

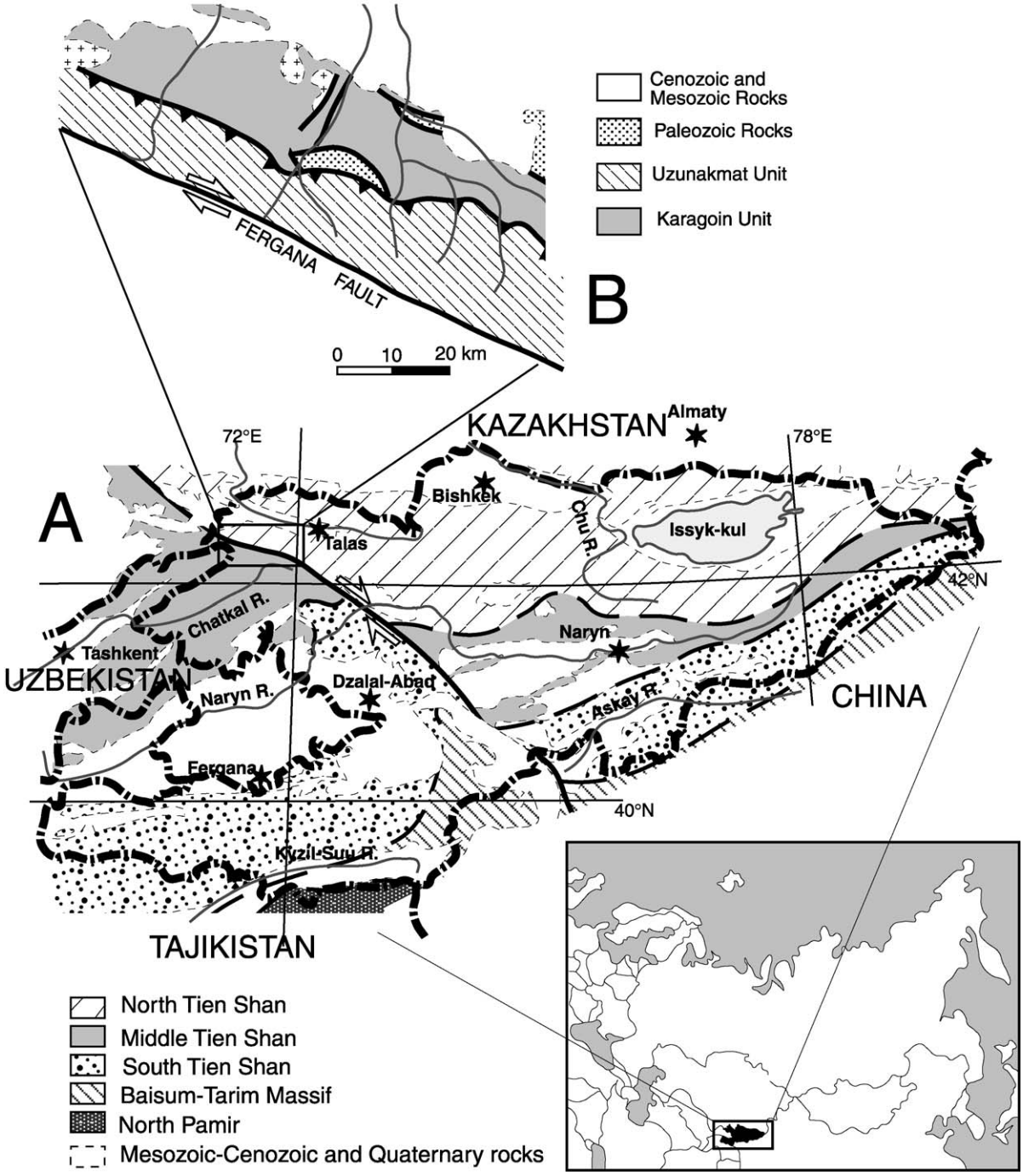

Fig. 1. (A) Location of the main geological domains within the Tien Shan Belt in the Kyrgyz Republic. (B) General geological map of the Talas Ala Tau depicting the two main sheets.

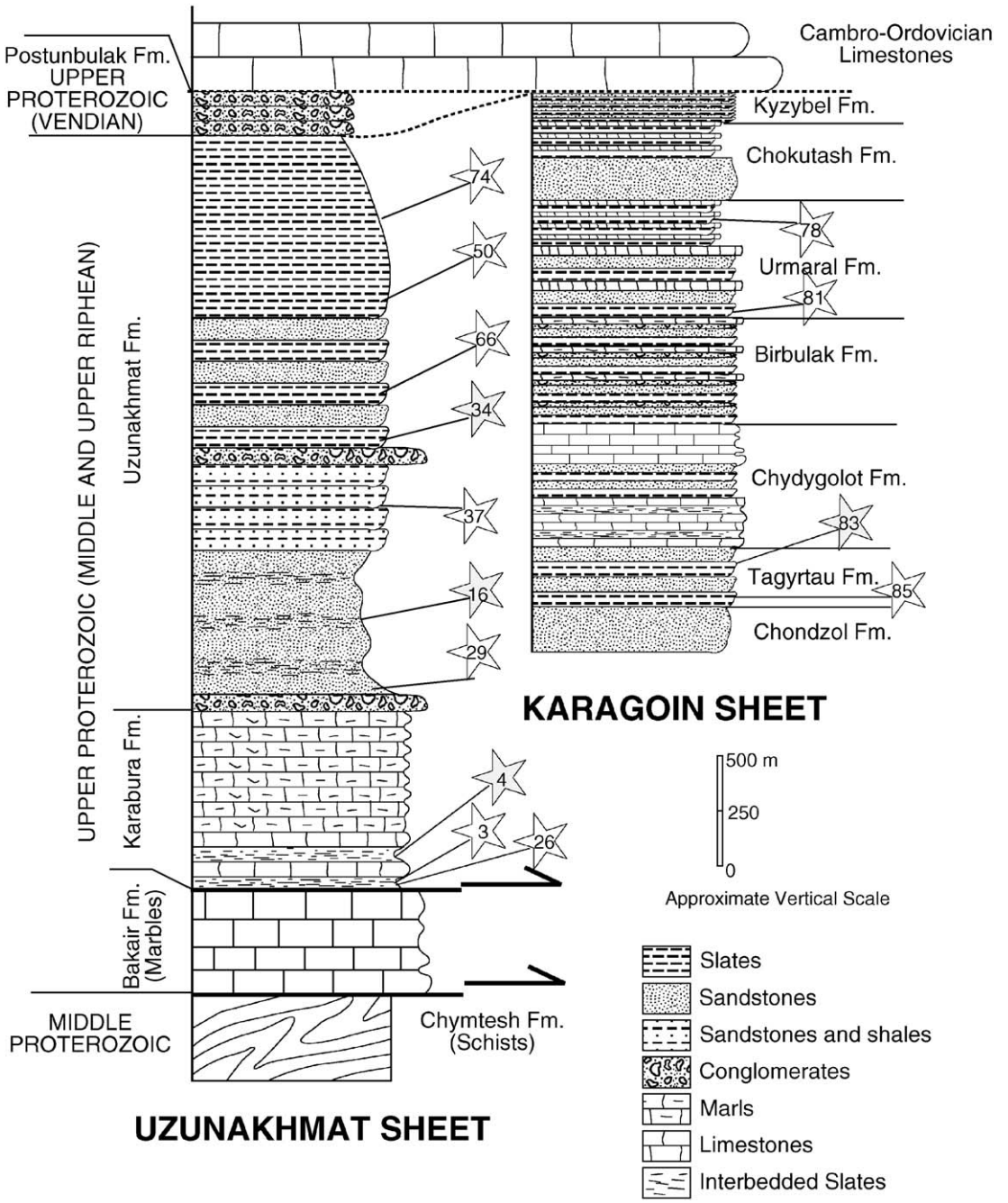

Fig. 2. Synthetic stratigraphy of the Talas Ala Tau in the Uzunakhmat and Karagoin sheets. The stars represent the stratigraphic location of the studied samples.

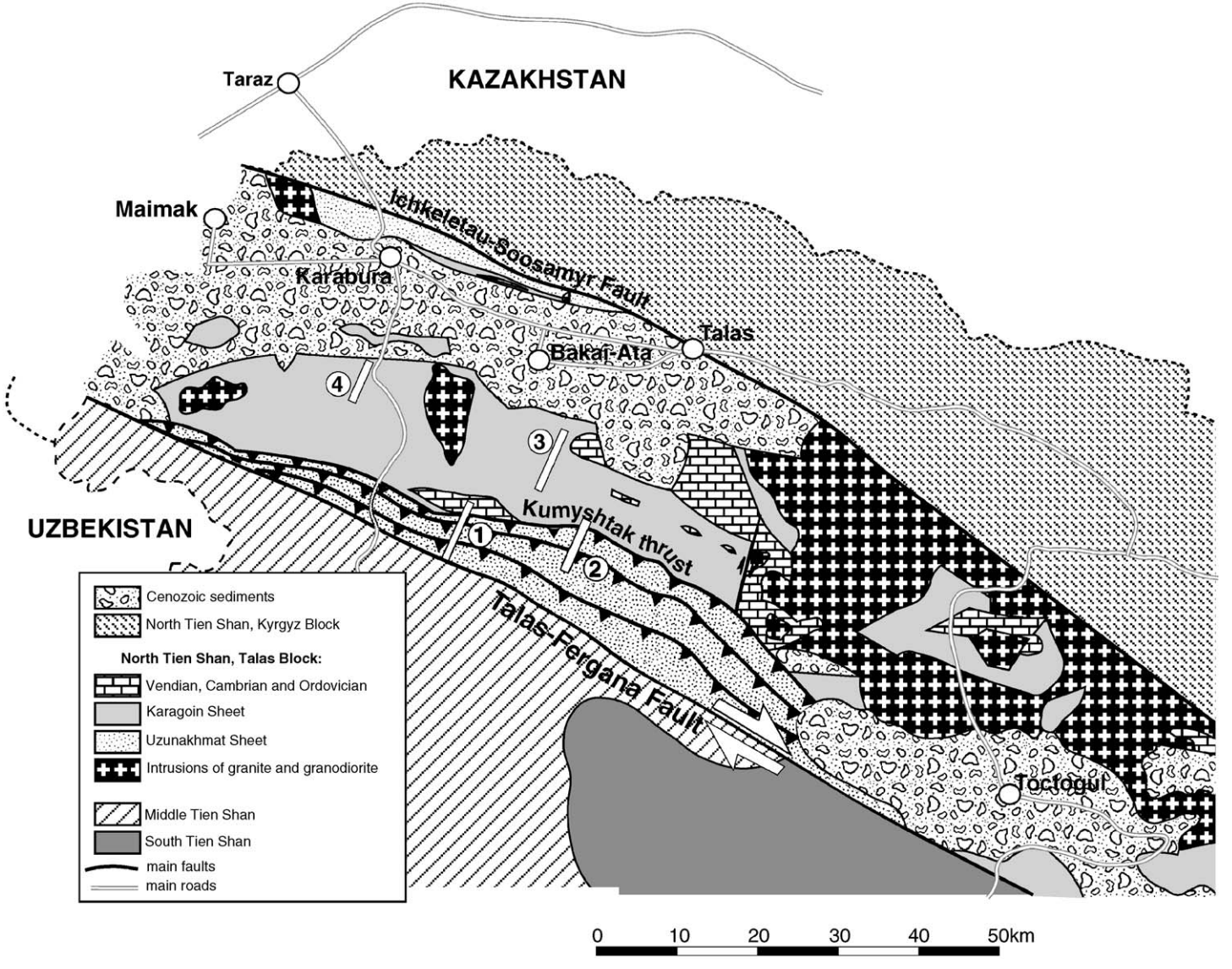

Fig. 3. General geological map of the Talas Ala Tau, indicating the location of the detailed cross-sections used to construct the general cross-section: (1) Postunbulak; (2) Beskol; (3) Urmaral; (4) Karabura.

The Uzunakhmat sheet is composed by up to 3-km-thick sequence of the Bakair, Karabura and Uzunakhmat formations of Lower to Middle Riphean age (Kiselev and Korolev, 1981), while the Karagoin group is composed from bottom to top by Chondzol, Tagyrtau, Chydygolot, Birbulak, Urmaral, Chokutash and Kyzylbel formations (Maksumova, 1980) (Fig. 2).

Within the Talas Ala Tau, all the aforementioned formations are unconformably overlain by Ordovician limestones. The deformation causing such the deformation fossilized by the mentioned unconformity can be interpreted to be related to the ones described by Allen et al. (2001). Subsequently, the Lower Paleozoic rocks were generally slightly folded

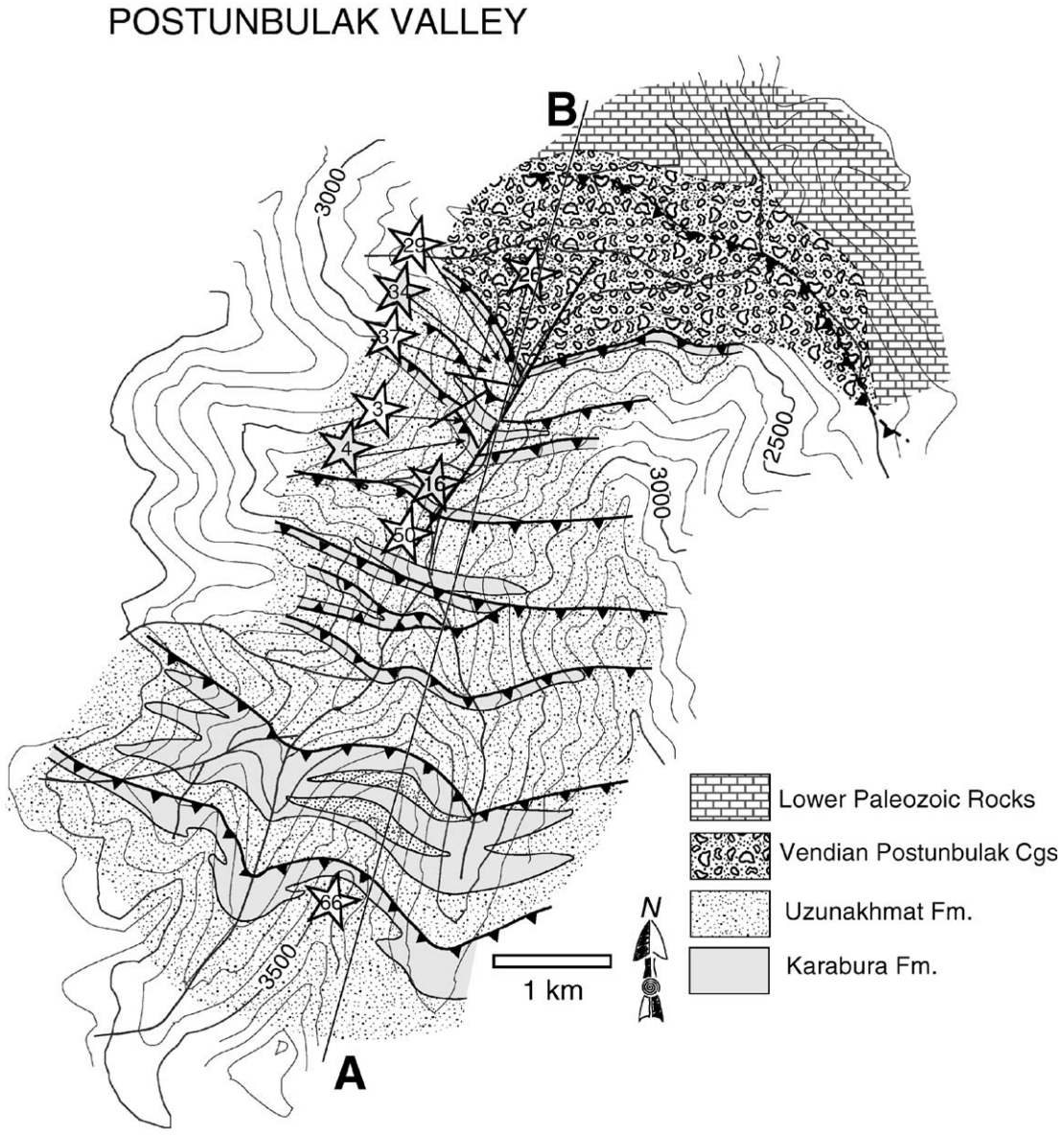

Fig. 4. Geological map of the Postunbulak Valley depicting the typical fold-and-thrust belt map pattern. Location of samples in the Uzunakhmat sheet is shown. A–B indicates the trace of the cross-section in Fig. 5.

during the Uralian orogeny, when the granites present in the region were intruded (Fig. 3). Furthermore, during the Tertiary Himalayan deformation, and in addition to the uplift, part of the range was tilted and rotated resulting into a re-orientation of previous structures. This rotated the change in the dip sense of the pervasive Baikalian axial-plane foliation, previously misinterpreted as the result of the Talas basin closure with an apparent double vergence pattern (Khudoley, 1993).

The Talas Belt is limited to the southwest by the Talas–Fergana Fault (Figs. 1 and 3) (Burtman et al., 1996), a continental scale dextral strike slip fault with more than 220 km of displacement. The presence of such feature precludes the continuation of the structure to the south, making impossible any attempt to continue the studied cross-section in that direction.

Regarding the metamorphism of the region, there are no detailed studies on its characteristics, only some references indicate the greenschist facies of the Uzunakhmat sheet with increasing grade to the south (Forlova, 1982) while the Karagoin sheet was considered unmetamorphosed.

3. The Talas Ala Tau cross-section

A field campaign was carried out in the region resulting in the construction of a geological map of the whole region (Fig. 3) completed with detailed maps of representative areas of the style and type of deformation of the region as well as cross-sections. Sampling was collected along NE–SW valleys running transverse to the strike of the main structures, which trend approximately NW–SE. The studied valleys were Postunbulak, where most of the samples were collected (Figs. 4 and 5, number 1 in Fig. 3), and Beshkol, Urmaral and Karabura (Fig. 6, numbers 2, 3

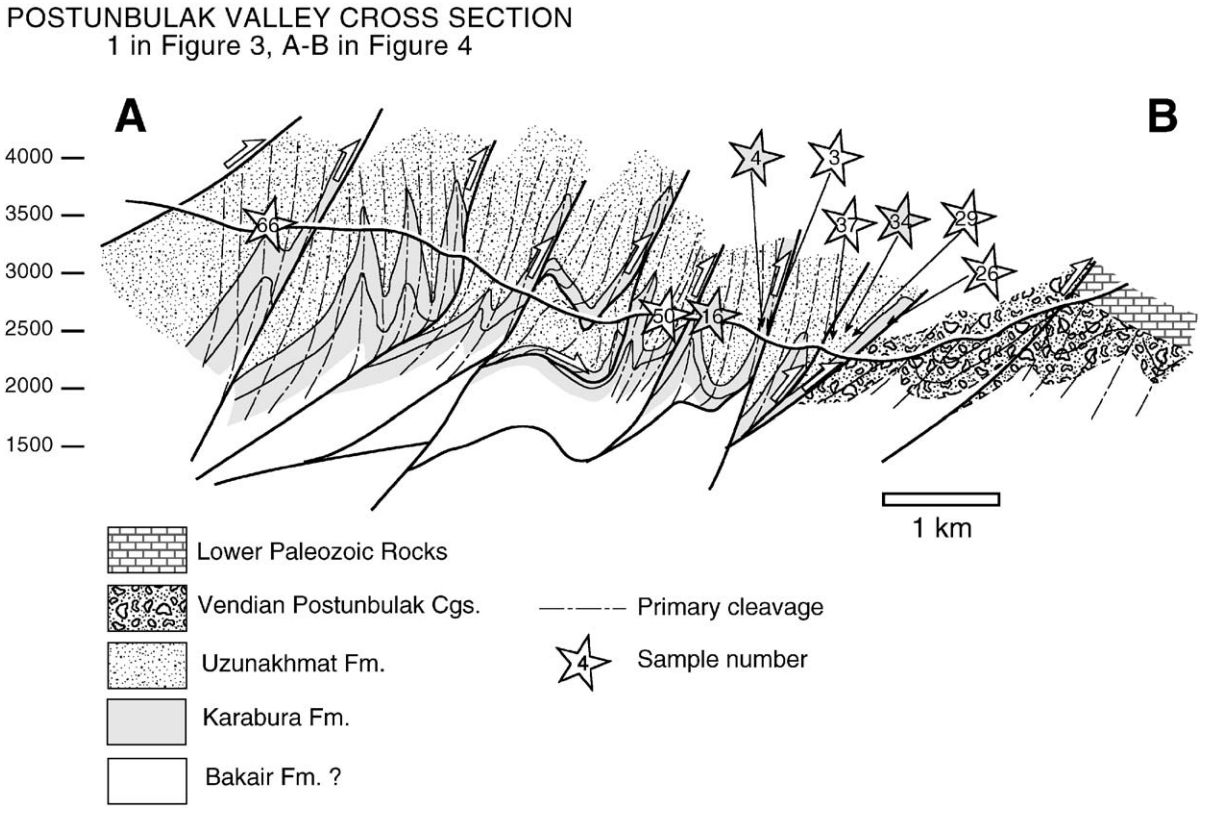

Fig. 5. Cross-section of the Uzunakhmat sheet in the Postunbulak Valley. Samples are projected onto the cross-section surface.

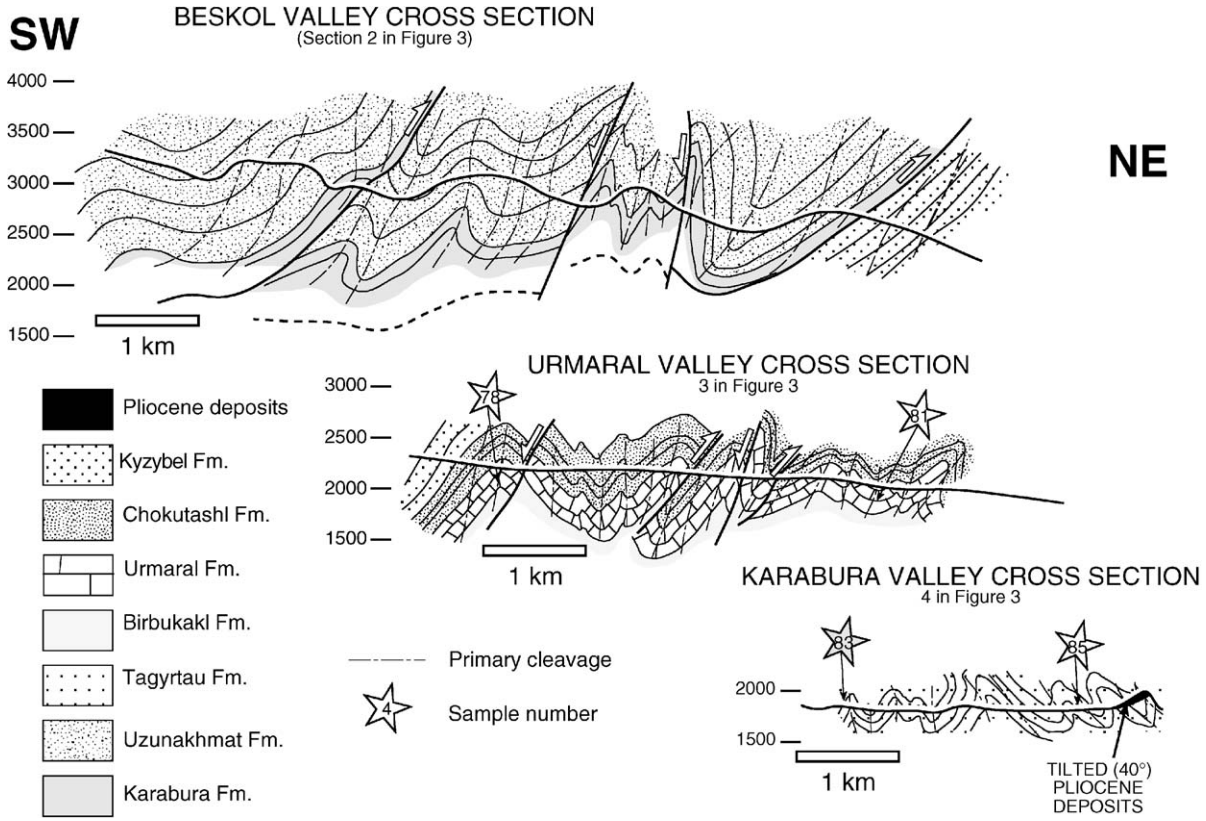

Fig. 6. Cross-sections of the Beskol (Uzunakhmat sheet), Urmaral and Karabura Valleys (Karagoin sheet) and location of part of the studied samples.

and 4, respectively, in Fig. 3). The geological profiles where chosen in order to build up a composite cross-section representative of the main structure of the Talas Ala Tau (Fig. 7).

Based on our structural study, three main deformation events can be recognized. The most recent deformation corresponds to the Himalayan event, responsible for the uplift and the tilting of the most recent Pliocene continental sediments of the area. No ductile deformation can be related to this event even at a local scale. The Uralian deformation event, which is the most prominent in most of Tien Shan, is of relatively low intensity. We can only identify open folds within the Paleozoic rocks and which do not impart pervasive cleavage. These Uralian folds are also interpreted to fold previous structures that will be later described.

The most prominent and important deformation event affecting the studied rocks was of Precambrian age associated to the Baikalian orogeny. Evidences of this age arise from the fact that the pervasive cleavage found in the Precambrian rocks (Riphean and Vendian) is never found in the Lower Paleozoic (Cambro-Ordovician) ones. In addition, the folds, and even the thrusts, found along the constructed cross-sections are overlain unconformably by the same Lower Paleozoic rocks.

3.1. The folds and the axial-plane cleavage

Folds are the most important structures in the region (Fig. 8A); they show a kilometer long wavelength and are cut by faults. There is a clear tendency to be more acute (closer) to the SW and more open towards the NE. They all present horizontal or subhorizontal fold axis that can be traced for long distances (π diagrams in Fig. 9A,B and fold axis in C). The axial planes strike parallel to the ranges (NW to SE) but their dip changes from SW dipping in the

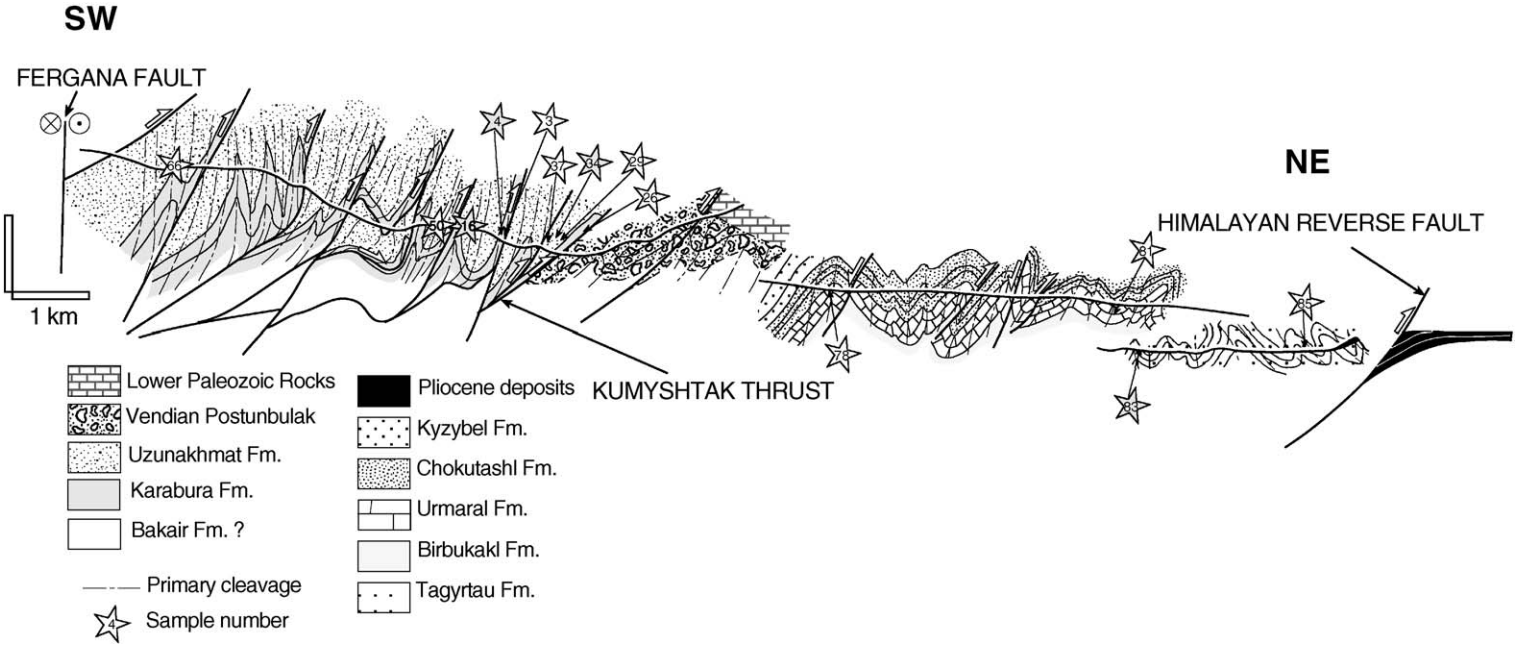

Fig. 7. Composite cross-section of the Talas Ala Tau indicating the relationships of the different units and sections studied.

SW of the studied units to vertical and even NE dipping towards the NE caused by the rotation induced by the reverse faults, as seen in outcrop scale folds found in the Tagyrtau Formation (Figs. 6 and 8B). Axial planes are always marked by a pervasive cleavage (Fig. 8C) mostly vertical or subvertical (Fig. 9D and E) that increases gradually its penetrativity from NE to SW. Depending on the nature of the

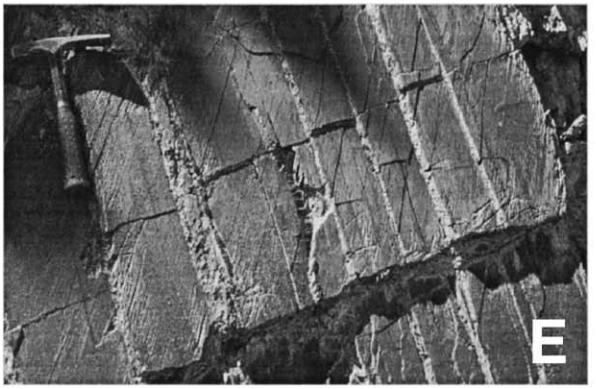

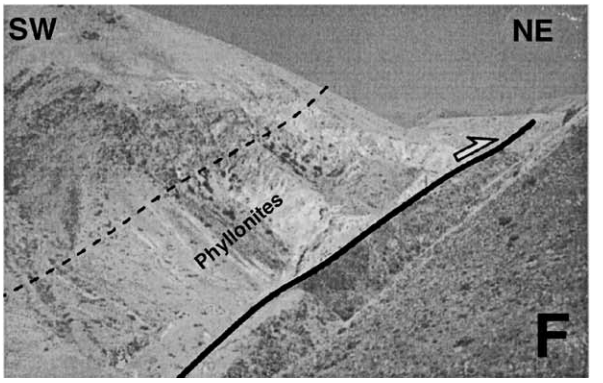

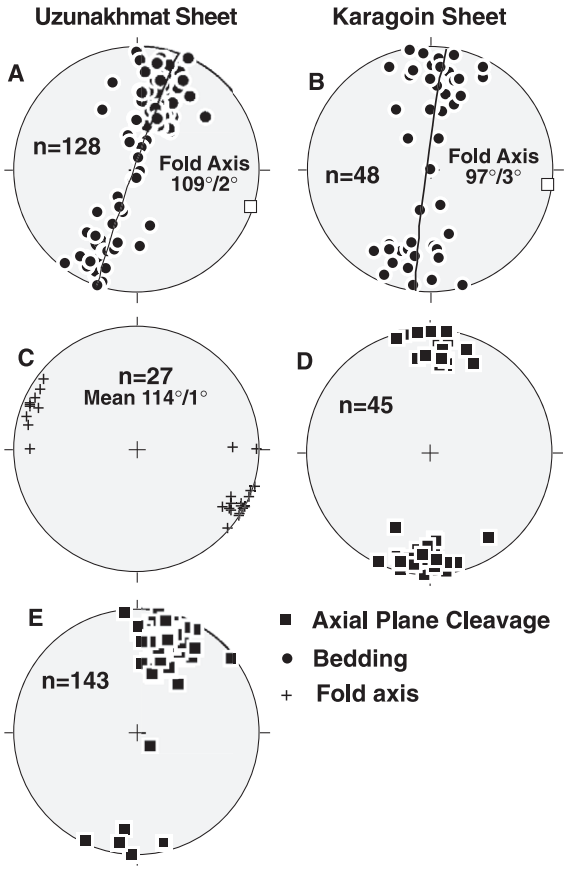

Fig. 9. Stereonets, Schmidt projection, lower hemisphere, showing the orientation of the geometric elements identified in the folds of the Talas Ala Tau. Explanation is found in the text.

affected rocks, the role of the pressure solution in the genesis of this structure changes drastically. While in the limestones, it is hard to identify cleavage planes, shortening is accumulated by developing mullions (Fig. 8D) which are evidence of important layer-parallel shortening caused by the strong viscosity contrast between the limestones and the surrounding fine-grained detrital rocks.

The cleavage in the fine-grained detrital rocks is pervasive and very penetrative (Fig. 8E) although penetrativity decreases qualitatively from SW to NE along the cross-section. The cleavage ranges from a slaty cleavage to a rough slaty cleavage within the fine-grained rocks while it is a rough cleavage in the sandstones. A good description of the nature, origin and the processes involved in the genesis of the axial-plane cleavage in the sandstones is shown in Becker (1995).

3.2. The faults

Related to the more prominent folds described above, or cross-cutting them, there is a large number of faults with different displacements and ages. In addition to the Fergana Fault, already described, the geometry of most of the faults can be interpreted as thrusts causing fault-bend and fault-propagation folds. From the direct observation and from the construction of the cross-sections, it can be noted that most of the faults in the area, specially in the Uzunakhmat sheet, can be traced following surfaces that run, at least partially, parallel to bedding surfaces corresponding to the lower part of the Karabura Formation and develop a penetrative phyllonitic cleavage in the hangingwall parallel to the fault surface (Fig. 10A). Furthermore, some of the folds previously described can be interpreted to be originated as fault-bend folds developed above ramps or related to higher shear strain rates in the overturned limbs of folds. Another striking fact is the abundance of fault rocks in the hangingwall of the mentioned faults, which can be up to 200 m thick in the Kumyshtak Thrust (Fig. 8F). The fault rocks consist of intensely foliated phyllonites and minor amounts of crush breccias. The phyllonites are

Fig. 8. (A) Photo of the NW slope of Postunbulak Valley where the existence and geometry of the folds is evidenced. Axial planes dip toward the SW. Vertical relief is approximately 1500 m. The folds correspond to those represented in the SW limit of the cross-section in Figs. 5 and 7. (B) Fold in the Tagyrtau Formation with its axial plane dipping to the NE due to the tilting caused by the recent Himalayan deformation. (C) Axial-plane cleavage in the hinge of a major fold in the Postunbulak Valley. The rocks correspond to the basal levels of the Uzunakhmat Formation. Note the pervasiveness and penetrativity of the cleavage, especially in the finest-grained beds. (D) Layer-parallel shortening processes in the carbonates of the Karabura Formation. Note the mullions developed in the most competent bed, while less competent beds do not develop folding. Coin for scale is 2.5 cm in diameter. (E) Slaty cleavage developed in the finest-grained rocks of the Uzunakhmat Formation. Note the angle between cleavage and bedding. (F) Trace of the Kumyshtak Thrust in the NW slope of the Postunbulak Valley overthrusting the Uzunakhmat sheet on top of the Karagoing sheet. The phyllonites in the hangingwall are approximately 130 m thick.

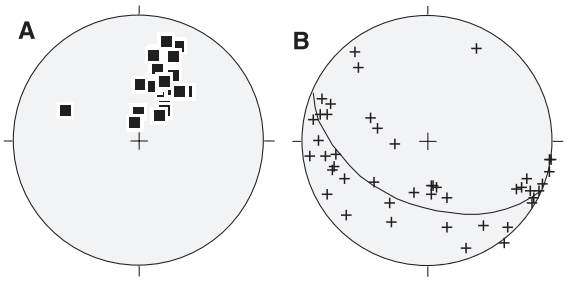

Fig. 10. Stereonets, Schmidt projection, lower hemisphere. (A) Black squares represent poles to the orientation of the phyllonitic cleavage. (B) The crosses depict the fold axis orientation of the folds related to the hangingwall shear zones of the main thrusts in the Uzunakhmat sheet. Note that they fit along the marked great circle, which is parallel to the phyllonitic cleavage, suggesting the presence of curved hinges.

intensely folded with small-scale folds that depict varied axial orientations following a great circle coincident with the orientation of the phyllonitic cleavage (Fig. 10B). This disposition of the fold axis indicates the curved shape of their hinges, which characterizes the hangingwall shear zone. The phyllonitic foliation is oblique to the axial-plane foliation previously described and parallels the thrust surfaces although it is intensely folded locally, probably in response to Uralian or Himalayan reactivations of the thrust surfaces.

4. Sampling strategy

Fourteen samples of slates were collected along the studied cross-section in order to record any variations in metamorphic grade across the whole range using the illite crystallinity technique (Kübler, 1968) and to establish the metamorphic conditions. Different kinds of foliations, axial planar and phyllonitic, were sampled. Nine samples were studied in more detail by SEM and TEM techniques to have a deep understanding on the nature and origin of the metamorphic phyllosilicates.

Samples were collected in the Karabura (3), Uzunakhmat (7), Tagyrtau (2) and Urmaral (2) formations and are representative of the whole cross-section of the region (Fig. 7). The three samples from the Karabura Formation (3, 4 and 26) were collected in the phyllonitized interbedded slates close to the Kumyshtak thrust, while the rest of the slates were collected in places where the main foliation was parallel to the axial planes of the folds.

5. Methods

5.1. X-ray diffraction

X-ray diffraction studies were carried out using a Philips PW 1710 Powder Diffractometer with Cu-Ka radiation, graphite monochromator and automatic divergence slit. The <2-μm fraction was separated by centrifugation. Oriented aggregates were prepared by sedimentation on glass slides. Preparation of samples and experimental conditions for illite crystallinity measurements were carried out according to IGCP 294 IC Working Group recommendations (Kisch, 1991). Our measurements (y) were transformed into CIS values (x) according to the equation $y=0.707x+0.0034$ ($r=0.999$), obtained in our laboratory using the international standards of Warr and Rice (1994). The b cell-parameter of micas and chlorites was obtained from the (060) peak measured on slices of rock cut normal to the main foliation of the samples (Sassi and Scolari, 1974). For all the spacing measurements, quartz from the sample itself was used as internal standard.

5.2. Scanning electron microscopy (SEM) and high-resolution transmission electron microscopy (HRTEM)

Following XRD results and optical microscopy study, most of the samples were prepared as thin sections orientated approximately normal to the dominant planar fabric, with epoxy resin and carbon-coated for examining by SEM, using back-scattered electron (BSE) imaging and energy-dispersive X-ray (EDX) analysis to obtain textural and chemical information. These observations were performed using a Zeiss DSM 950 SEM at the C.I.C. (Universidad de Granada), equipped with an X-ray Link Analytical QX-20 energy-dispersive system (EDX). An accelerating voltage of 20 kV, with a beam current of 1–2 nA and counting time of 100 s, was used to analyze the phyllosilicates by SEM, using both natural and synthetic standards: albite (Na), periclase (Mg), wollas-

tonite (Si and Ca), orthoclase (K) and synthetic Al_2O_3 (Al), Fe_2O_3 (Fe), and $MnTiO_3$ (Ti and Mn).

The structural formulas of micas were calculated on the basis of 22 negative charges $O_{10}(OH)_2$. Although these analytical techniques cannot distinguish between Fe^{3+} and Fe^{2+}, Guidotti et al. (1994) showed that even in low redox parageneses, approximately 50% of Fe in muscovite is Fe^{3+} and values close to 85% can be reached in oxidizing environments. Therefore, in the formula calculations, it has been assumed that 75% of the Fe in micas is Fe^{3+}. The chlorite formulas were calculated on the basis of 28 negative charges.

Table 1
Crystal-chemical parameters and bulk mineralogy determined by XRD

Samples	White mica		Mineral composition
	b	KI < 2 μm	Ms, Qtz, Chl (all samples)
Uzunakhmat sheet			
Uzunakhmat Formation			
66	9.037	0.26	Cc, K-fs, Ilm, Rt, Zrn
74	9.030	0.22	Cc, K-fs
50	9.035	0.25	Pg, Cc, Pl
16	9.033	0.23	Pl
Karabura Formation			
3*	9.038	0.33	Cc, Pl, Ilm
4*	9.009, 9.023	0.32	Ank, Pl, Fe-ox., Ap, Mnz
Uzunakhmat Formation			
37	9.031	0.27	Ill/Pg, K-fs
34	9.027	0.26	Cc, Dol, Pl, Fe-ox.
29	9.023	0.29	Cc, K-fs
Karabura Formation			
26*	9.020	0.32	Cc, Fe-ox., Ilm, Zrn
Karagoin sheet			
Urmaral Formation			
78	–	0.36	Cc, Ap
81	9.042	0.36	Cc, Pl, K-fs
Tagyrtau Formation			
83	–	0.30	Cc, Sm, Pl, K-fs, Fe-ox., Mn-ox.
85	–	0.27	Cc, Pl

Mineral abbreviations according to Kretz (1983). In bold, samples studied by TEM.
Samples with an asterisk are the phyllonites. Ill/Pg = Na–K mica, Fe-ox. = iron oxide, Mn-ox. = manganese oxide, Sm = smectite.

Due to the very fine-grained nature of these samples, the spatial resolution of the textural features obtained using the optical and SEM microscopy is not enough to resolve all the matrix characteristics. Therefore, four samples representative of the Talas Ala Tau cross-section were selected for HRTEM study: sample 83 (Karagoin sheet) and samples 34, 4 and 16 (Uzunakhmat sheet). They have been selected in the light of their tectonostratigraphic positions (Fig. 7) and their crystal-chemical parameters (Table 1). Thin sections were prepared with Canada Balsam. HRTEM observations were obtained with a Philips CM20 (STEM) located at the C.I.C. and equipped with an EDAX solid-state EDX detector, operating at 200 kV, with a LaB_6 filament and a spatial resolution of 2.7 Å between points and 1.4 Å between fringes.

6. Results

6.1. Bulk-rock analyses

Whole-rock analyses of the major elements (Table 2, deposited) were carried out using X-ray fluorescence (XRF). Major-element data show average values similar to the upper continental crust and the average of Post-Archean Australian Shales (PAAS) published by Taylor and McLennan (1985) and commonly used as reference shales.

6.2. Mineralogy and crystal-chemical parameters

The XRD results are depicted in Table 1.

For both the Uzunakhmat and Karagoin sheets, the bulk mineralogy determined by XRD and investigated further by SEM mainly comprises quartz, phyllosilicates (micas and chlorite) and feldspars. Accessory minerals include iron oxides, rutile, illmenite, zircon and apatite.

The illite crystallinity results (Kübler Index, hereafter KI) indicate that all the studied samples fall in very low-grade metamorphic conditions (0.36 to 0.22Δ° 2θ) corresponding to anchizonal and epizonal grades (according to Merriman and Peacor, 1999). The lowest metamorphic grade is found in the youngest rocks (which are also the most exter-

Table 2
Whole-rock analyses of major elements (oxide wt.%)

Samples	SiO_2	Al_2O_3	CaO	MgO	Na_2O	K_2O	Fe O	Fe_2O_3	MnO	TiO_2	P_2O_5	LOI	SUM
Uzunakhmat sheet													
66	66.76	10.31	4.40	1.61	2.05	2.10	0.58	4.05	0.10	0.99	0.14	5.40	98.50
74	65.65	9.78	3.83	2.76	2.62	1.50	0.45	4.19	0.38	0.56	0.14	7.01	98.88
50	69.97	11.62	0.97	2.14	2.28	2.00	0.23	5.38	0.10	1.07	0.14	2.72	98.61
16	55.63	19.27	0.25	3.92	0.85	4.80	1.65	6.28	0.11	0.94	0.14	3.46	97.30
3	61.28	17.51	0.17	3.33	0.62	4.93	0.02	6.11	0.11	0.81	0.12	3.51	98.52
4	59.58	21.73	0.50	1.33	0.47	6.19	1.13	2.35	0.02	1.05	0.17	3.87	98.39
37	70.22	12.38	0.44	2.52	1.62	2.39	0.30	5.33	0.07	0.65	0.14	2.73	98.79
34	62.88	10.73	6.01	2.10	1.57	2.05	1.28	3.83	0.26	0.66	0.16	6.83	98.36
29	58.47	17.92	0.19	2.90	1.31	4.26	4.31	2.83	0.06	0.79	0.14	4.32	97.50
26	71.24	9.91	1.82	1.47	2.29	1.63	2.14	2.44	0.73	0.57	0.14	3.67	98.06
Karagoin sheet													
81	69.53	13.03	2.05	2.11	2.25	3.13	0.53	2.55	0.04	0.36	0.07	3.75	99.40
83	67.94	11.43	2.61	2.20	0.65	1.96	1.24	4.43	0.05	0.77	0.15	4.92	98.34

nal ones), those of the Urmaral Formation in the Karagoin sheet. In turn, the highest ones (0.26–0.23Δ° 2θ) correspond to the rocks situated to the SW in the Uzunakhmat Formation, in the most internal zone of the cross-section. Their KI values indicate high-anchizone–epizone conditions. Other KI values for samples from the Uzunakhmat Formation, located eastward, depict a lower metamorphic grade (0.29–0.26Δ° 2θ, high anchizone) consistent with a steady increase in metamorphic grade during the generation of the folds to the SW in accordance with the strain increase seen by the higher cleavage intensities.

In contrast with the KI values found in the Uzunakhmat Formation, those in the phyllonites of the Karabura Formation are consistently higher (0.32–0.33Δ° 2θ), despite their deeper position. The relation of these values with another type of cleavage, which is related to the thrusts development, seems to indicate high strain rates that in fault zones can be responsible of the development of intense deformation characteristics in the mica crystals (see Electron microscopy observations and analysis (SEM and TEM) and Discussion).

The samples from the Urmaral Formation, within the Karagoin sheet, depict values that reach the low-anchizone range (0.36Δ° 2θ). Because they correspond to cooler conditions than those recorded in older rocks of the same unit (0.27–0.30Δ° 2θ, in the Tagyrtau Formation), the origin of these changes may be related to deformation at shallow depths.

The KI values of the whole samples (not shown) are generally close to the KI of the <2-μm fractions, therefore, the effect of detrital micas must be minimal.

In contrast with other collisional belts, the anchizone–epizone limit does not appear to coincide with the onset of widespread cleavage (e.g. Gutiérrez-Alonso and Nieto, 1996). On the contrary, cleavage is very well developed throughout the very low-grade metamorphic conditions, suggesting another deformation environment for the Talas Ala Tau Proterozoic rocks.

Another of the white mica crystal-chemical parameters measured was the *b* cell-parameter. The results obtained show consistent values between 9.023 and 9.042 Å (Table 1). Fig. 11 shows an almost perfect correlation ($r=0.95$) between the *b* parameter and phengitic content of micas of these rocks. Therefore, both parameters can be used to evaluate the minimum pressure reached by the rocks (Massone and Scherreyer, 1987).

6.3. Electron microscopy observations and analyses (SEM and TEM)

6.3.1. Textures

The textural aspect of these rocks is generally homogeneous, although there are notable differences

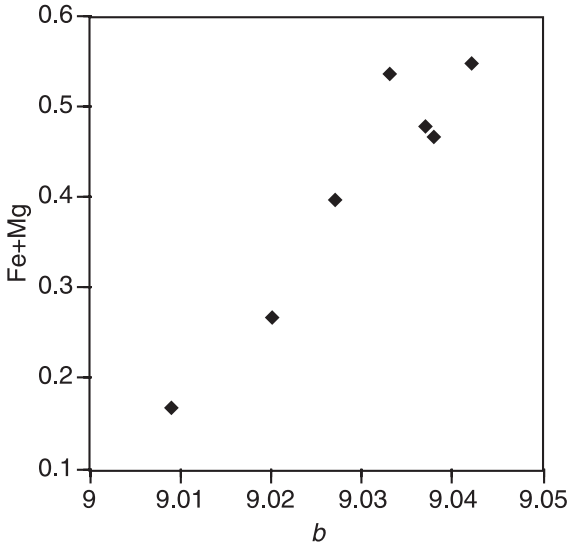

Fig. 11. Correlation between *b* parameter (Å) and Fe + Mg (a.f.u.) in micas.

between the samples belonging to the Karagoin and Uzunakhmat sheets.

The most characteristic feature of the Karagoin rocks is the ubiquitous presence of phyllosilicate intergrowths up to 300 μm in length and 200 μm in width. Similar stacks have frequently been described in anchizone environments, under incipient metamorphic conditions (Milodowsky and Zalasiewicz, 1991; Li et al., 1994). Mostly, they are formed by Fe-rich chlorite and white mica (Fig. 12A, B and C), often showing a very fine intergrowth not recognizable at SEM resolution. In some cases, they are very elongated, with curved borders and even broken, as in Fig. 12B. There are ellipsoidal and equidimensional stacks as well. Most packets are intergrown subparallel to (001), some appearing as wedges, forming semi-coherent boundaries with neighbouring crystals, frequently oriented at a low angle to the mineral cleavage. In fact, they show textures (such as microfolds) and morphologies that appear to be detrital in origin but the phyllosilicates association is consistent with metamorphic processes.

Two populations of intergrown K dioctahedral micas have been recognized within the stacks. Fig. 12C reveals different contrasts for phengitic (lighter) and muscovitic (darker) micas. The less phengitic micas overgrow the more phengitic ones.

Generally, the Karagoin rocks comprise a framework, of angular quartz grains (20–40 μm) and a very fine-grained matrix (< 5 μm) mainly composed of micas and chlorite, calcite, K-feldspar, albite and Fe and Mn-oxides.

In the Uzunakhmat rocks, there are large amounts of phyllosilicates, responsible for a well-developed slaty cleavage. These samples contain larger crystallites than the Karagoin ones, in coherence with the KI parameter previously described. Although the lithologies are similar, they differ slightly in grain size, with samples 34 and 66 (similar KI) containing phyllosilicates no more than 20 μm in thickness (Fig. 12D). In contrast, phyllonitic samples 3 and 26 contain grains under 5–10 μm (Fig. 12E). As well, in samples 66 and 50, chlorite–white mica intergrowths have been described, similar to those in the Karagoin rocks.

The textural aspect of phyllonitic slate sample 4 is clearly different (Fig. 12F), with a high mica content and nodules composed of phyllosilicate rims and quartz cores with a rotated structure very similar to macroscopic structures of tectonic origin described in the field.

The mineral composition of these rocks is very similar to the Karagoin ones with illmenite, Ti-oxides (rutile?), zircon and sporadic dolomite (sample 34) as well as ankerite in veins (sample 4) as accessory minerals.

At the lattice scale, sample 83 (Karagoin Group) shows packets of phyllosilicates no more than 700 Å in thickness. Fig. 13A and B shows the typical texture at TEM scale of an anchizonal rock composed mostly of phyllosilicates. Chlorite packets present microfolds normal to the lattice-fringes (Fig. 13B) and interstratified individual 7-Å layers, which in some areas form small packets containing no more than three layers (Fig. 13A). In relation to the dioctahedral K-rich mica, the most notable feature is the mottled texture. In Fig. 13B, we have also observed several mica packets that are oblique to the other phyllosilicate crystals whose borders seem to have been dragged during slip along crystal boundaries. Polytypes are 2M for mica and semi-random for chlorite.

Samples 34 and 16 (Uzunakhmat Group) belong to the same formation but are situated in different tectonic units (see Figs. 4 and 5). In general, they are both

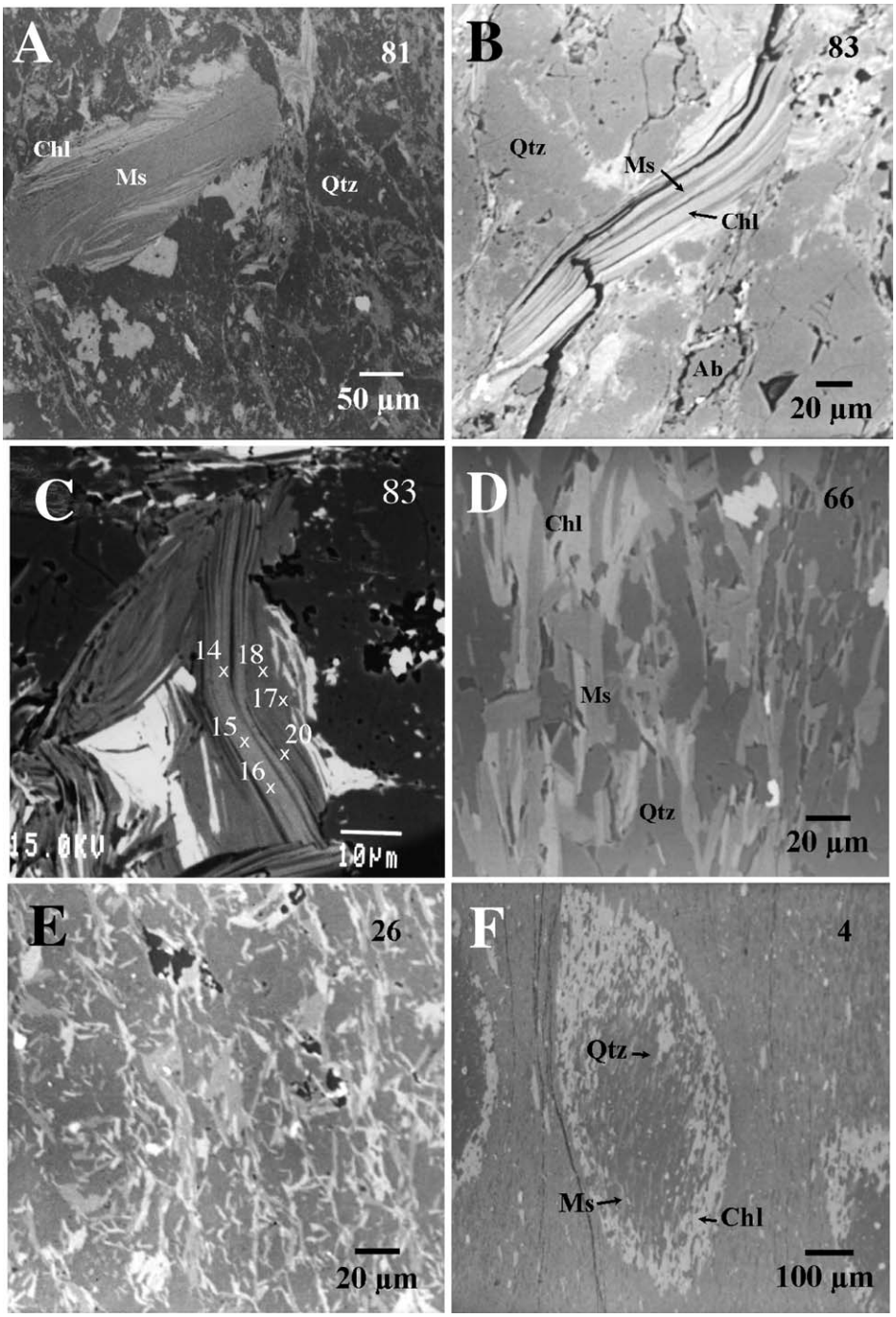

Fig. 12. Back-scattered electron images showing texture of the samples: (A) Fine-grained matrix of sample 81 with an elongated stack mostly comprising white mica. (B) Broken stack formed of chlorite and muscovite with an elongated and slightly folded shape in sample 83. (C) Stack of sample 83 showing two generations of micas. Analyses 14, 15 and 16 show higher phengitic and ferrimuscovitic contents than analyses 17, 18 and 20. (D) Crystalline aspect of sample 66, mainly consisting of mica, chlorite and quartz. (E) Texture of sample 26, with well-developed slaty cleavage and abundant phyllosilicate crystals (mica and chlorite). (F) Sample 4 shows nodules as in the image, within very fine-grained surroundings.

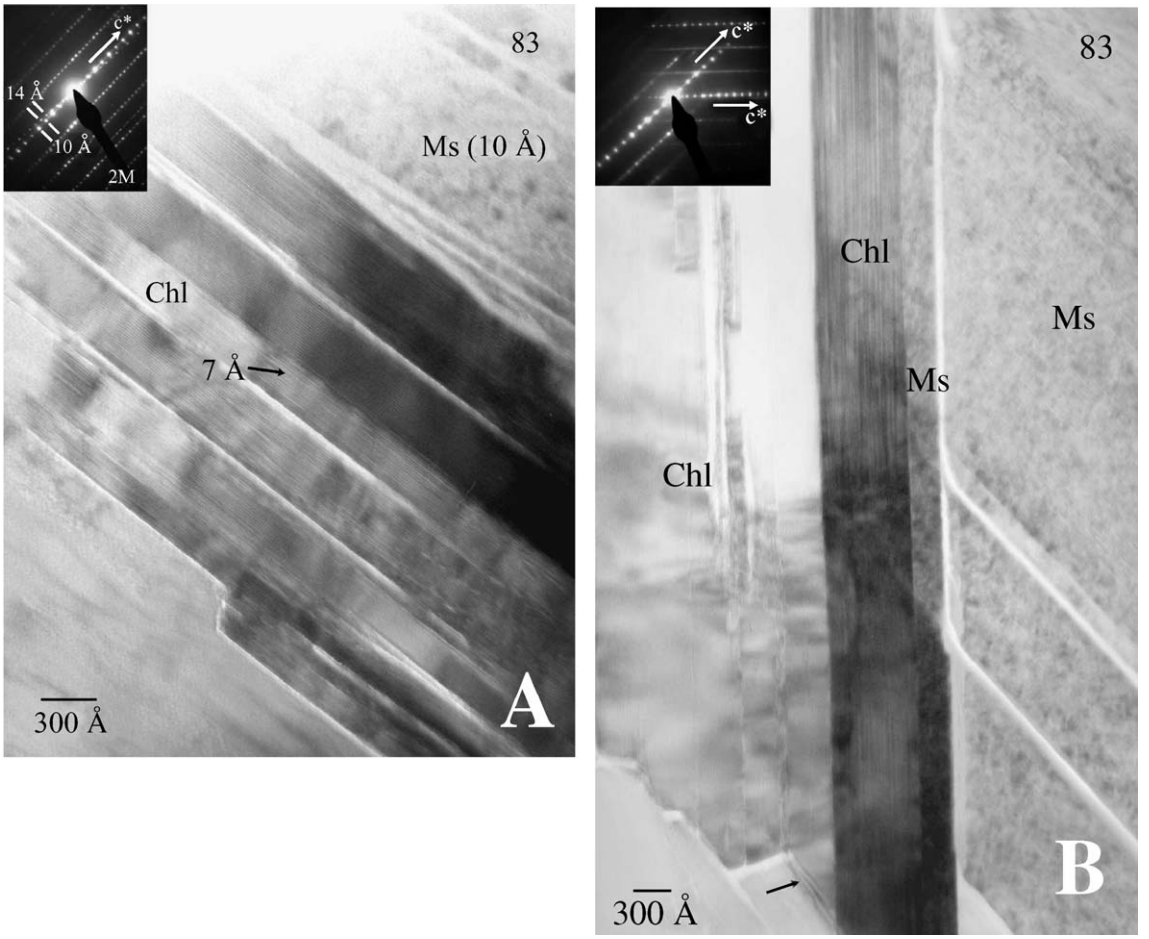

Fig. 13. Lattice-fringe images of sample 83 (Karagoin sheet). (A) Chlorite and mica defect-free crystals, with only slightly bended layers or microfolds in the first ones, where lower periodicities (i.e. 7 Å) have also been detected. Most of the crystals are thinner than 500 Å. Both mica reflections (2M polytype) and chlorite are present in the SAED. (B) Packets of mica oblique to other mica and chlorite crystals, which show similar characteristics to those described in A.

characterized by defect-free phyllosilicate packets (muscovite and chlorite) with well-defined boundaries >1000 Å in thickness and with the sporadic presence of microkinks in chlorites and a mottled texture in mica (Fig. 14A and B). In both samples, there are superperiodicities in the chlorites, which are various multiples of 14 Å, revealing the presence of a long-range stacking order (Fig. 14B).

The phyllonitic sample 4 (Uzunakhmat Group), despite being characterized by thick 2M muscovite packets with well-defined boundaries, shows an intense mottled texture, highly damaged and defective, with frequent layer terminations and changes in contrast (Fig. 15).

6.4. Chemical composition of phyllosilicates

The chemical composition of the phyllosilicates was determined by EDX on the SEM.

6.5. Dioctahedral micas

The structural formulas of representative K dioctahedral micas normalized to $O_{10}(OH)_2$ are presented in

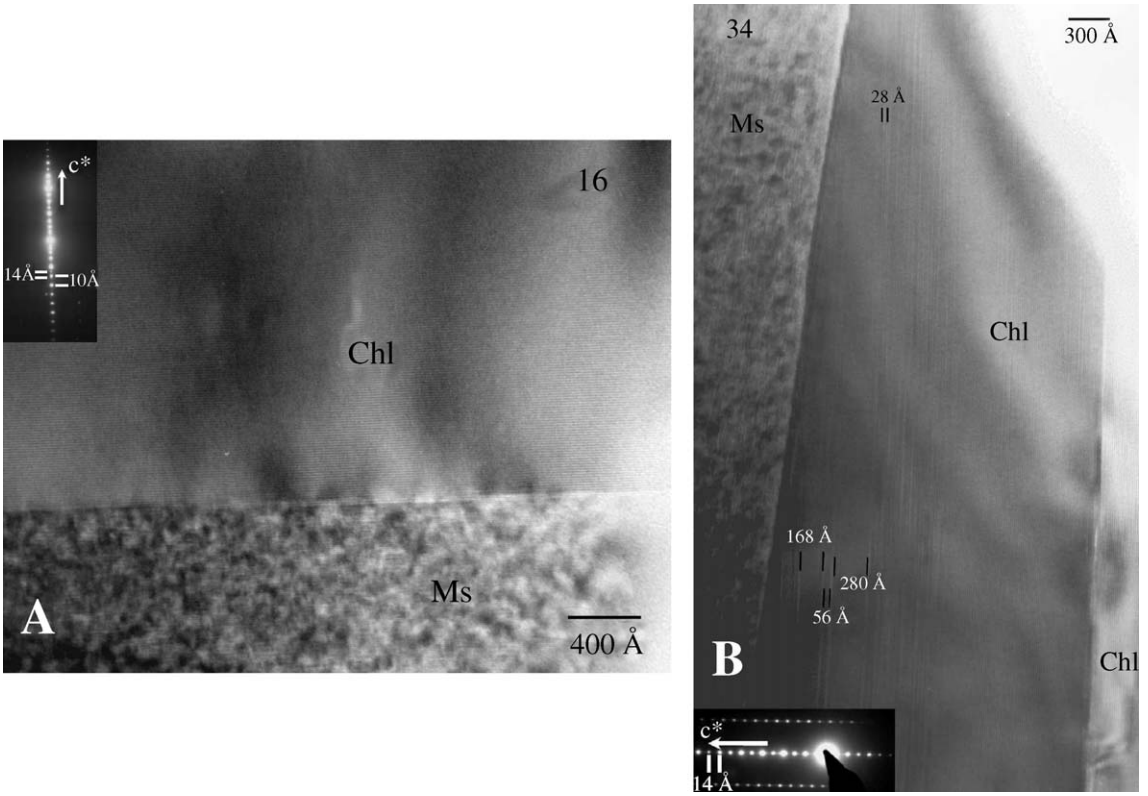

Fig. 14. (A) Lattice-fringe image of sample 16 with well-developed phyllosilicate crystals (chorite and mica). (B) Lattice-fringe image of sample 34 which shows a thick chlorite crystal having high periodicities as well as a mica crystal (phengite).

Table 3. The results indicate a lack of chemical homogeneity in the contents of the distinct chemical elements, due not only to differences among samples (Fig. 16, see, for instance, that Si = 3–3.6 a.f.u., Fe + Mg = 0.1–0.6 a.f.u. or Al = 1.8–2.75 a.f.u.), but also evident within individual samples (Table 3, see, for example, Si = 3.1–3.6 a.f.u. and Al = 1.8–2.5 a.f.u. for sample 81 or Si = 3.1–3.5 a.f.u. and Al = 2–2.75 a.f.u. for sample 26).

Each chemical parameter is affected by several compositional vectors (Fig. 16). No correlation between the interlayer population and Si exist ($r = -0.41$) which means a lack of significant illitic substitution (Fig. 16A). Most of the analyses present a K content of >0.85 a.f.u. Fig. 16B shows the effect of the ferrimuscovitic vector. This vector significantly affects the chemical variables represented in Fig. 16C and D, which show the phengitic tendency. This is the main vector determining the proportions of Si, Al and Fe + Mg, but these chemical parameters are also affected by the ferrimuscovitic vector and to a small extent by the illitic one.

Nevertheless, the analyses corresponding to the phyllonitic samples (3, 4 and 26) define a tendency closer to the theoretical phengitic vector than the common slates, and a behavior which is less affected by the ferrimuscovitic vector (see Fig. 16C and D). The correlation between Si and Fe + Mg is clearly much higher in the K-micas of the phyllonites ($r = 0.91$) than in the slates ($r = 0.56$). In addition, the sum of octahedral cations in the K-micas of the phyllonitic samples becomes slightly lower than 2 a.f.u. when 75% of the iron is considered as Fe^{3+} (Table 3), that is, this assumption is not completely valid for phyllonitic samples. All of these

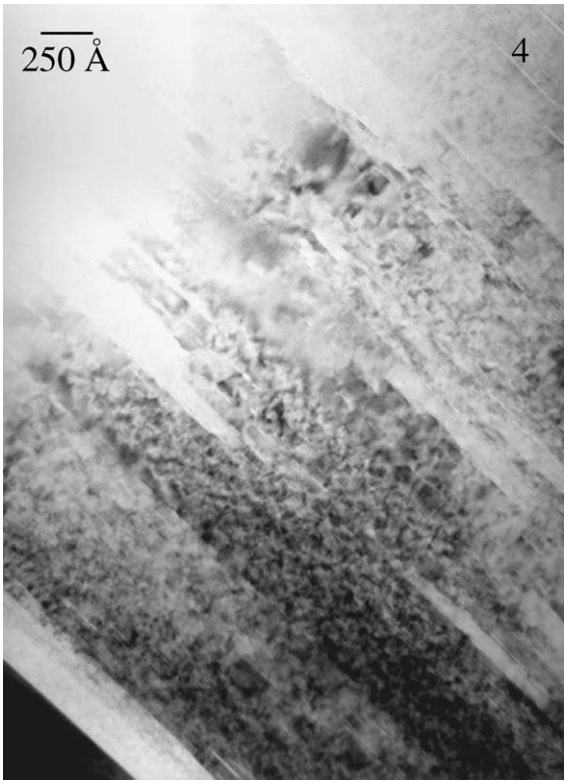

Fig. 15. Low-magnification image of sample 4 (phyllonite) of muscovitic packets with an intense mottled texture and frequent change of contrast normal to the fringes.

characteristics show that the phyllonites definitely show a lower ferrimuscovitic content than the slates.

Mn and Ca (also analyzed) are not included in the data table as Mn is absent and Ca is only significant in micas of sample 78. Na is either absent or present in proportions of ≤ 0.12 a.f.u., and therefore, parago-

Table 3
Representative structural formula for micas normalized to $O_{10}(OH)_2$

Analysis	Si	^{IV}Al	^{VI}Al	Fe	Mg	Ti	$^{VI}\Sigma$	K	Na	Σ inter.
66/2	3.23	0.77	1.56	0.27	0.15	0.03	2.01	0.92	0.00	0.92
66/5	3.36	0.64	1.44	0.33	0.20	0.03	2.00	0.90	0.00	0.90
66/7	3.30	0.70	1.37	0.40	0.22	0.02	2.02	0.90	0.04	0.95
66/8	3.47	0.53	1.55	0.15	0.27	0.01	1.98	0.88	0.00	0.88
66/9	3.23	0.77	1.51	0.31	0.16	0.03	2.01	0.92	0.04	0.95
66/11	3.26	0.74	1.51	0.29	0.18	0.02	2.01	0.90	0.04	0.93

Table 3 (*continued*)

Analysis	Si	^{IV}Al	^{VI}Al	Fe	Mg	Ti	$^{VI}\Sigma$	K	Na	Σ inter.
66/12	3.32	0.68	1.60	0.12	0.27	0.02	2.00	0.94	0.00	0.94
16/1	3.45	0.55	1.53	0.24	0.19	0.03	1.99	0.80	0.00	0.80
16/3	3.27	0.73	1.58	0.21	0.21	0.03	2.03	0.88	0.00	0.88
16/6	3.21	0.79	1.45	0.31	0.26	0.04	2.06	0.87	0.04	0.91
16/8	3.30	0.70	1.52	0.22	0.24	0.04	2.02	0.89	0.00	0.89
16/11	3.26	0.74	1.53	0.28	0.20	0.03	2.04	0.86	0.00	0.86
3 2	3.50	0.50	1.49	0.20	0.27	0.02	1.98	0.84	0.00	0.84
3 3	3.50	0.50	1.49	0.18	0.28	0.02	1.97	0.84	0.04	0.88
3 4	3.43	0.57	1.51	0.20	0.23	0.03	1.97	0.87	0.04	0.91
3 5	3.51	0.49	1.40	0.28	0.32	0.02	2.03	0.69	0.07	0.76
3 6	3.31	0.69	1.57	0.21	0.22	0.02	2.02	0.87	0.00	0.87
3 7	3.41	0.59	1.57	0.16	0.23	0.02	1.98	0.88	0.00	0.88
4 2	3.13	0.87	1.89	0.06	0.05	0.01	2.00	0.86	0.05	0.91
4 3	3.07	0.93	1.83	0.04	0.04	0.08	2.00	0.83	0.08	0.91
4 4	3.26	0.74	1.81	0.07	0.06	0.03	1.97	0.82	0.06	0.88
4 7	3.13	0.87	1.89	0.05	0.06	0.01	2.01	0.84	0.07	0.91
4 8	3.28	0.72	1.71	0.14	0.12	0.02	1.98	0.85	0.05	0.90
4 10	3.15	0.85	1.81	0.09	0.07	0.03	1.99	0.88	0.04	0.93
4 12	3.18	0.82	1.78	0.13	0.09	0.02	2.02	0.87	0.00	0.87
34/1	3.23	0.77	1.53	0.23	0.19	0.05	2.00	0.89	0.07	0.96
34/2	3.29	0.71	1.58	0.19	0.21	0.02	2.00	0.96	0.00	0.96
34/4	3.37	0.63	1.57	0.19	0.21	0.02	2.00	0.87	0.00	0.87
34/5	3.32	0.68	1.62	0.17	0.17	0.03	1.99	0.88	0.00	0.88
34/7	3.28	0.72	1.52	0.27	0.25	0.02	2.06	0.84	0.00	0.84
34/9	3.21	0.79	1.67	0.18	0.15	0.03	2.02	0.87	0.03	0.90
26/5	3.29	0.71	1.66	0.14	0.18	0.01	2.00	0.91	0.00	0.91
26/6	3.18	0.82	1.70	0.15	0.13	0.03	2.00	0.91	0.05	0.96
26/7	3.28	0.72	1.69	0.12	0.14	0.03	1.97	0.89	0.04	0.93
26/8	3.07	0.93	1.83	0.08	0.06	0.04	2.01	0.85	0.09	0.95
26/10	3.31	0.69	1.66	0.14	0.16	0.02	1.97	0.89	0.07	0.96
26/12	3.51	0.49	1.54	0.17	0.25	0.02	1.97	0.84	0.00	0.84
26/14	3.25	0.75	1.77	0.11	0.11	0.00	1.99	0.93	0.00	0.93
26/15	3.39	0.61	1.68	0.13	0.13	0.02	1.96	0.83	0.06	0.88
78/1	3.17	0.83	1.64	0.18	0.19	0.01	2.03	0.73	0.12	0.99
78/2	3.14	0.86	1.88	0.05	0.05	0.01	1.99	0.67	0.23	0.94
78/3	3.35	0.65	1.58	0.14	0.28	0.03	2.03	0.80	0.00	0.84
78/4	3.21	0.79	1.80	0.09	0.11	0.01	2.01	0.80	0.04	0.87
78/7	3.34	0.66	1.61	0.12	0.25	0.01	1.99	0.86	0.06	0.95
78/11	3.24	0.76	1.73	0.10	0.14	0.02	1.98	0.83	0.10	0.95
78/12	3.10	0.90	1.71	0.18	0.09	0.02	1.99	0.92	0.04	1.02
78/13	3.05	0.95	1.67	0.06	0.06	0.16	1.96	0.86	0.07	0.98
81/2	3.52	0.48	1.32	0.30	0.35	0.01	1.98	0.94	0.00	0.94
81/3	3.42	0.58	1.39	0.26	0.38	0.01	2.04	0.90	0.00	0.90
81/4	3.49	0.51	1.40	0.22	0.36	0.01	2.00	0.92	0.00	0.92
81/5	3.13	0.87	1.59	0.23	0.14	0.05	2.01	0.87	0.11	0.98
81/8	3.34	0.66	1.43	0.27	0.26	0.04	2.00	0.96	0.00	0.96
81/9	3.45	0.55	1.47	0.18	0.32	0.01	1.99	0.91	0.04	0.95
83/2	3.24	0.76	1.62	0.24	0.17	0.03	2.06	0.77	0.00	0.78
83/3	3.26	0.74	1.64	0.20	0.22	0.01	2.06	0.80	0.00	0.80
83/5	3.23	0.77	1.45	0.35	0.16	0.06	2.05	0.85	0.00	0.85
83/6	3.37	0.63	1.37	0.31	0.28	0.05	2.02	0.88	0.00	0.88
83/7	3.49	0.51	1.58	0.19	0.20	0.01	1.99	0.75	0.03	0.79
83/8	3.25	0.75	1.39	0.36	0.21	0.07	2.02	0.92	0.00	0.92

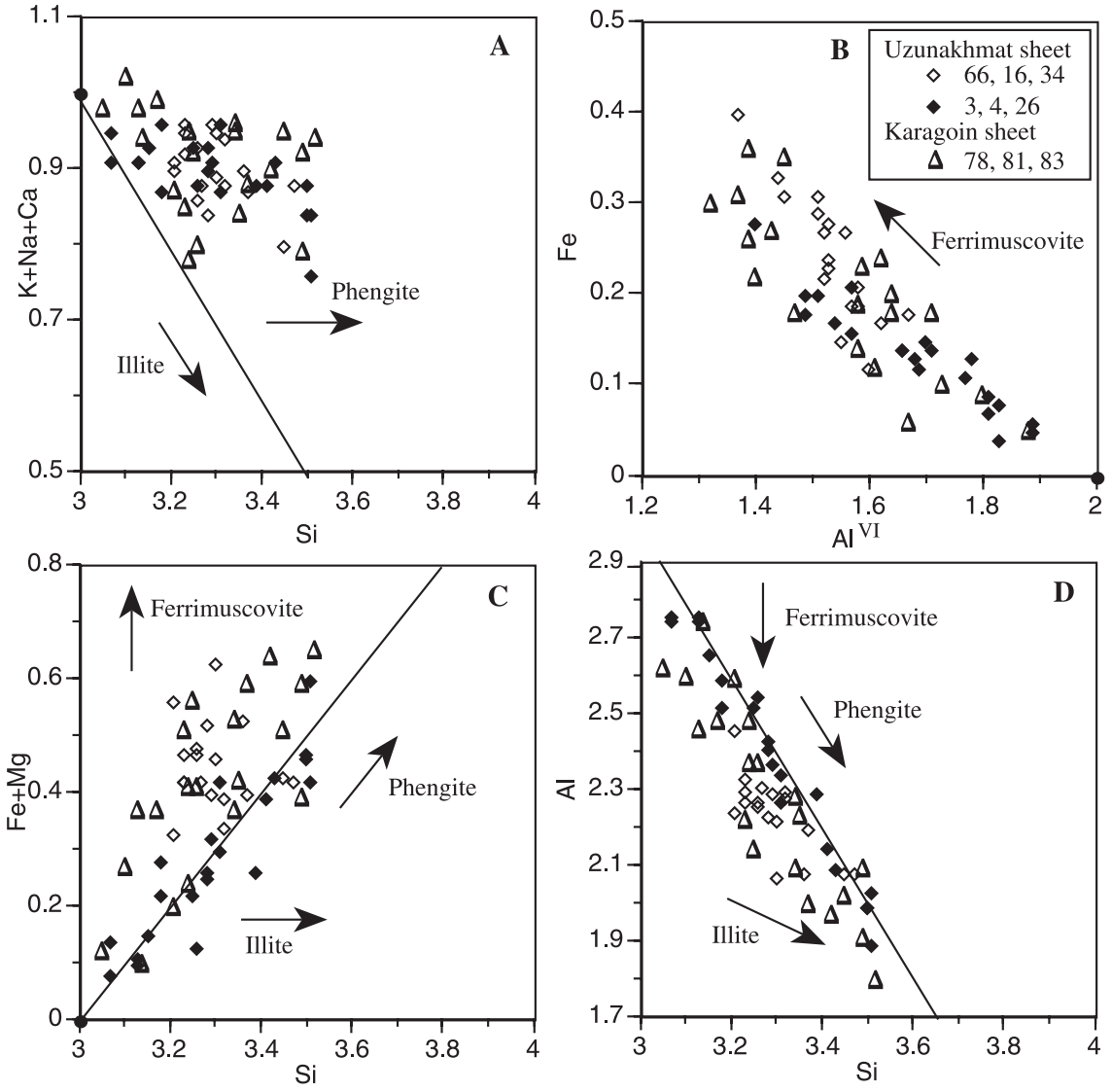

Fig. 16. Chemical composition diagrams of micas of the studied samples, black points and solid lines respectively indicate the theoretical muscovite position and corresponding exchange vectors. Open symbols have been used for shales and solid symbols for phyllonites.

nitic substitution is not a significant compositional vector in these samples, except for samples 50 and 37, which contain paragonite and Na–K mica, respectively (Table 1). Albite is present as a metamorphic phase, which, in addition to the low-temperature conditions, must be responsible for both the lack of paragonite in most of the samples as a discrete phase and the scarcity of paragonitic substitution in the K-micas.

6.6. Chlorite

Trioctahedral chlorites have been analyzed (Table 4, deposited) and correspond to the chamosite variety. The Fe/(Fe + Mg) ratios do not define a clear trend throughout the sequence, being almost constant and within the range of values characteristic of chlorites in low-grade metamorphic rocks. The difference between the ^{VI}Al and the ^{IV}Al is also characteristic of chlorites

Table 4
Chemical compositions for chlorites normalized to $O_{10}(OH)_8$

	Si	^{IV}Al	^{VI}Al	Fe	Mg	Mn	Ti	$^{VI}\Sigma$	Fe/(Fe+Mg)
Uzunakhmat sheet									
66 1	2.69	1.31	1.35	2.74	1.88	0.00	0.00	5.98	0.59
66 2	2.82	1.18	1.36	2.74	1.81	0.00	0.00	5.91	0.60
66 3	2.80	1.20	1.32	2.75	1.88	0.00	0.00	5.94	0.59
3 1	2.84	1.16	1.36	2.45	2.06	0.03	0.00	5.90	0.54
4 1	2.76	1.24	1.51	2.87	1.44	0.00	0.02	5.85	0.67
4 2	2.68	1.32	1.40	3.00	1.54	0.00	0.01	5.95	0.66
4 3	2.77	1.23	1.44	2.95	1.50	0.00	0.00	5.90	0.66
4 4	2.68	1.32	1.47	3.02	1.42	0.00	0.00	5.92	0.68
34 2	2.79	1.21	1.33	2.72	1.88	0.01	0.00	5.94	0.59
34 3	2.79	1.21	1.34	2.69	1.86	0.02	0.01	5.93	0.59
34 4	2.66	1.34	1.47	2.78	1.66	0.02	0.00	5.93	0.63
26 1	2.68	1.32	1.50	2.72	1.70	0.00	0.00	5.91	0.62
26 4	2.88	1.12	1.29	2.62	1.98	0.02	0.00	5.91	0.57
Karagoin sheet									
81 3	2.95	1.05	1.24	2.28	2.37	0.00	0.01	5.90	0.49
83 2	2.83	1.17	1.41	2.31	2.13	0.03	0.00	5.88	0.52
83 3	2.80	1.20	1.54	2.63	1.67	0.00	0.00	5.83	0.61

that developed in this type of environment (Li et al., 1994). There are no differences between the chlorite compositions of phyllonites and that of the slates.

7. Discussion

7.1. Geotectonic setting of Talas Ala-Tau. Alpine vs. accretionary subduction-related environment

Merriman and Frey (1999) described specific patterns of very low-grade metamorphism that are essential to distinguish among various geotectonic settings in the absence of higher-grade metamorphic rocks according to Robinson (1987). Maruyama et al. (1996) recognized two types of collisional settings: (1) Alpine settings, involving the subduction of continental margin assemblages beneath another continent, which produce rocks that pass into intermediate pressure-type Barrovian sequences; (2) accretionary settings, generated by the subduction of oceanic crust, which produce a steep $P–T–t$ path through the subgreenschist to blueschist facies field. Nevertheless, the establishment of metamorphic paths in very low-grade sequences is not an easy task as textural relations between minerals are not obvious. A combination of structural analysis and a detailed study of phyllosilicates from samples taken along the Talas Ala Tau cross-section has allowed us to relate these data with the geological processes in order to deduce its geotectonic setting.

The KI values and the lack of chemical homogeneity in micas indicate a very low-grade metamorphic environment with a slight increase from low anchizone in the Karagoin sheet to high anchizone–epizone in the deepest samples of the Uzunakhmat sheet, that is, the most internal ones. The comparison of TEM images (Figs. 13 and 14) has revealed textural evidence of the different metamorphic grades. Such differences are not so obvious in the BSE images (Fig. 12), due to the inherent lower resolution of such images.

The KI is directly related to the size and crystallinity (number of defects) of the mica packets (Merriman and Peacor, 1999). As a consequence, it is a good estimate of the reaction progress in low- or very low-grade rocks. TEM study has shown a clear textural difference at lattice level between samples with higher or lower KI parameters (Figs. 13 vs. 14); therefore, KI differences can be confidently related with metamorphic grade.

The presence of mica–chlorite stacks in several samples (Fig. 12) is also typical of anchizone or low-grade epizone. Their origin has been much disputed in recent years by different authors (Dimberline, 1986; Milodowsky and Zalasiewicz, 1991; Li et al., 1994, among others). Giorgetti et al. (1997) interpreted that they are the result of mineral crystallization during the metamorphic event on previous detrital grains. Although the morphologies of the stacks must be inherited, the mineral composition is typical of very low-grade metamorphism and the texture of these stacks is in some cases very complex given that they are probably the result of different diagenetic–metamorphic and tectonic episodes.

Stacks sometimes include a very complex metamorphic phyllosilicate paragenesis (Giorgetti et al., 1997). In the phyllosilicate stacks of Talas, an intergrowth of two different populations of micas, phengites and muscovites has been detected (Fig. 12C). Both populations of micas are obviously in disequilibrium and represent two different steps of crystallization during the geological evolution of the Talas rocks. The phengitic laths are abundant and usually strained, whereas the muscovitic ones are less frequent and sometimes located in narrow voids. Textural observa-

tions suggest that the phengitic laths correspond to a previous episode, while the growth of muscovitic ones must have been later. The phengitic content of micas is related to their crystallization pressure (Massone and Scherreyer, 1987). According to these authors, in the absence of a limiting assemblage, the phengitic content of micas coexisting with a Mg, Fe silicate, as in the Talas rocks, can be used to derive minimum formation pressures for the enclosing rock. Therefore, both populations of micas give us information about the minimum pressure of two different times in the decompression path of Talas.

Dalla Torre et al. (1996) also found phengitic micas, corresponding to a HP/LT metamorphic event in the Franciscan Formation, overgrown by muscovitic micas assumed to correspond to a lower-pressure overprint. Micas from the Franciscan Formation presented KI corresponding to high-anchizone and low-epizone conditions, as do the Talas rocks. This history of mica crystallization throughout a decompression process could be responsible for the huge range of phengitic contents at individual sample level (Table 3 and Fig. 16). Therefore, the straight line defined by the mica compositions, perfectly parallel to the phengitic vector (Fig. 16D) should be considered as a reflection of the decompression of the Talas rocks. According to Massone and Scherreyer (1987), corresponding extreme Si values could be used to deduce the minimum pressure conditions of a decompression path. At least some of the mica analyses reaching Si contents of around 3.5 a.f.u. (Table 3, e.g. 81/2 or 81/4), are free of illitic substitution, present octahedral sum equal or very near its theoretical value (2.0 a.f.u.) and do not show any sign of contamination by other phases, which in any case would produce a significant change in the octahedral sum. Since other mica substitutions are also absent, these micas can therefore be considered as indicators of lower-pressure stability limits, as any other high-pressure mineral phase (Massone and Scherreyer, 1987). According to these authors, an Si content equal to 3.5 a.f.u. represents at least 8 kbar (see Figs. 2 and 3 of their work).

Fig. 11 shows an excellent correlation between the *b* parameter and the average phengitic content of micas for each sample, allowing us to use the *b* parameter value in addition to the phengitic content as a reliable estimate of pressure of the metamorphic process. Nevertheless, a difference of meaning between both parameters should be taken into account, chemical analyses by SEM indicate individual grain formation conditions, whereas *b* parameter is related to an average compositions of the different mica grains within the same sample. Therefore, if we deduce the pressure from the *b* parameter (around 4–5 kbar, Guidotti and Sassi, 1986), it actually represents an average condition during the decompression path.

The KI, *b* and phengitic content results obtained in this work indicate that folds were generated under low to very low temperature (< 300 °C) and intermediate to high pressures. Such conditions are not typical of deformation in collisional orogenic belts, but rather of subduction-related complexes. Due to the Fergana fault, we cannot link these rocks to other subduction-related ones of the same age that would be located to the SW, making it difficult therefore to prove this relation. Nevertheless, the style of deformation can also be an argument in the interpretation of the geodynamic setting of the studied deformation. From this point of view, it is clear that the deformation style of the Talas Ala Tau is a fold-and-thrust belt. Fold-and-thrust belts occur in two settings, forelands to orogenic belts and accretionary prisms in subduction complexes. Due to the different metamorphic gradients (LT–LP in foreland settings and LT–HP–IP in subduction complexes, we can expect different structures within the belt, including a prominent slaty cleavage development, which occurs under very low-temperature conditions in a subduction-related environment. The slaty cleavage development, under the aforementioned conditions, is generally always missing in the foreland thrust-and-fold belts until the onset of epizone conditions. Furthermore, the fact that all the thrusts clearly postdate the folds and are developed under colder conditions may be another argument to interpret the origin of these structures within a subduction complex. In addition, in the foreland fold-and-thrust belts, the folds and faults occur simultaneously, except for some out-of-sequence thrusts, and their geometry is completely linked to each other, but this is not the case in Talas Ala Tau, which is another argument in favor of a subduction environment.

The results obtained in this work can be correlated with others found in the same environments in modern orogens that can be used as analogues. The Cenozoic subduction-related belts from Japan, for instance, depict very similar KI values and a very similar

structural grain (DiTullio et al., 1993; Hibbard et al., 1993; Kanemoto and Otsuka, 2000; Ujiie, 1997, KI = 0.31–0.42). Other comparable subduction-related accretionary prisms with similar KI and *b* parameter values can be found in eastern Australia (Offler et al., 1998, KI = 0.21–0.38 and *b* = 9.025) and NW China (Jiang and Lin, 2000). In all the aforementioned cases, the metamorphism related to the accretionary prism development and deformation matches the characteristics found in the Talas Ala Tau and, therefore, despite the lack of direct correlation with other elements of the alleged subduction complex, we propose that the deformation found in this region took place in such an environment. This interpretation sheds new light on our understanding of the early history of terrane amalgamation in Central Asia, intensely obscured by subsequent deformation events.

7.2. Differences between slates and phyllonites

The phyllonites show features as crystal-chemical parameters, textural characteristics and chemical composition of micas different to the rest of the samples, which are considered "common" slates. Sample 4, which has been selected for TEM study as representative of the phyllonites, is located in the hangingwall of a thrust and very near the thrust plane. Their mica crystals are heavily damaged and defective (Fig. 15) and consequently the KI ($0.32\Delta^\circ$ 2θ) is somewhat higher than those in corresponding slates. The fact that the rocks with the highest deformation are characterized by high KI values and defective texture suggests an important role of the tectonic stresses and a less relevant one related to the change in temperature along the progress of the metamorphism.

Giorgetti et al. (2000) proposed that where tectonic strain proceeds faster than recrystallization can take place, it would favor a reduction in phyllosilicate crystal size and therefore an increase in the KI values. Previous studies (see Merriman and Frey, 1999 for a review) had concluded that in deeply buried high-strain zones, thicker cystallites result from annealing of strained phyllosilicates. Nevertheless, in high-level shear zones, lattice strain is not recovered and anomalously small crystal sizes and defective textures occur. This seems to have been the case for the phyllonites of the Talas Ala Tau cross-section and the fundamental origin of the differences in KI and texture between the two types of lithologies. In conclusion, tectonic stress can produce two different kinds of effects on very low-grade metamorphic rocks depending on the rate of crystallization, that is, strain-related crystal size reduction or recovery of sub-grain boundaries, resulting in more crystalline samples.

Although the whole-rock compositions do not show significant differences among the samples (Table 2, deposited), chemical differences have been discerned between micas in slates and phyllonites, mostly related with the ferrimuscovitic vector (Fig. 16). While mica analyses from phyllonites (diamond symbols in Fig. 16) fit the theoretical phengitic vector quite well, those from slates also show a significant presence of ferrimuscovite. Guidotti et al. (1994) concluded that the Fe^{2+}/Fe^{3+} ratio in micas is independent of metamorphic grade and reflects the opaque mineral assemblage in the rock, that is, the relative proportion of ferrimuscovite in a particular mica must be a consequence of the relative availability of Fe^{3+}. Therefore, the circulation of fluids along the fractures related with the thrusts in deep, highly reductive conditions might have been responsible for the genesis of phyllonite mica in the absence of Fe^{3+}, contrasting with slates in which the lower fluid/rock ratio had prevented the original Fe^{2+}/Fe^{3+} ratio of the pelitic sediment to be changed.

These aforementioned differences confirm that mineral crystallization in very low-grade metamorphism is a complex process, dependent not only on temperature but also on other factors such as tectonic stress or fluids circulation.

Acknowledgements

We thank M.M. Abad Ortega and A. González from the Centro de Instrumentación Científica of the Universidad de Granada for their help with HRTEM and SEM work, respectively. We would like to acknowledge the work of C. Laurin in revising the English of this text. Thanks are extended to L. Warr and M. Allen for their critical reviews and very helpful comments and suggestions. Financial support was supplied by Research Project No. BT 2000–0582 and FPI research grant to I.A., both of the Spanish Ministry of Science and Technology and Research Group RNM-0179 of the Junta de Andalucía. Field work to G.G.A. was facilitated by Apex Asia, further support comes

from Research Project No. BTE2000-1490-C02-01 of the Spanish Ministry of Science and Technology. This contribution is part of project IGCP 453.

References

Abdrakhmatov, K.Y., Aldazhanov, S.A., Hager, B.H., Hamburger, M.W., Herring, T.A., Kalabaev, K.B., Makarov, V.I., Molnar, P., Panasyuk, S.V., Prilepin, M.T., Reilinger, R.E., Sadybakasov, I.S., Souter, B.J., Trapeznikov, Y.A., Tsurkov, V.Y., Zubobich, A.V., 1996. Relative recent construction of the Tien Shan inferred from GPS measurements of present day crustal deformation rates. Nature 384, 450–453.

Allen, M.B., Alsop, G.I., Zhemchuzhnikov, V.G., 2001. Dome and basin refolding and transpressive inversion along the Karatau fault system, southern Kazakhstan. Journal of the Geological Society (London) 158, 83–95.

Becker, A., 1995. Quartz pressure solution: influence of crystallographic orientation. Journal of Structural Geology 17 (10), 1395–1405.

Bullen, M.E., Burbank, D.W., Garver, J.I., Abdrakhmatov, K.Y., 2001. Late Cenozoic tectonic evolution of the northwestern Tien Shan: new age estimates for the initiation of mountain building. Geological Society of America Bulletin 113, 1544–1559.

Burtman, V.S., Skobelev, S.F., Molnar, P., 1996. Late Cenozoic slip on the Talas–Ferghana fault, the Tien Shan, Central Asia. Geological Society of America Bulletin 108, 1004–1021.

Dalla Torre, M., Livi, J.T.K., Veblen, D.R., Frey, M., 1996. White K-mica evolution from phengite to muscovite in shales and shale matrix melange, Diablo Range, California. Contributions to Mineralogy and Petrology 123, 390–405.

Dimberline, A.J., 1986. Electron microscope and microprobe analysis of chlorite–mica stacks in the Wenlock turbidites, mid Wales, UK. Geological Magazine 123, 299–306.

DiTullio, L., Laughland, M.M., Byrne, T., 1993. Thermal maturity and constraints from illite crystallinity and vitrinite reflectance in the shallow levels of an accretionary prism; Eocene–Oligocene Shimanto Belt, Southwest Japan. In: Underwood, M.B. (Ed.), Thermal Evolution of the Tertiary Shimanto Belt, Southwest Japan; An Example of Ridge–Trench Interaction. Special Paper - Geological Society of America, vol. 273, pp. 63–82.

Forlova, N.S., 1982. Influence of metamorphism on deformational properties of rocks (an example from Talas Ala Tau). Geotectonika 4, 18–24 (in Russian).

Frey, M., Teichmüller, M., Teichmüller, R., Mullis, J., Kuenzi, B., Breitschmid, A., Gruner, U., Schwizer, B., 1980. Very low-grade metamorphism in external parts of the Central Alps, illite "crystallinity", coal rank and fluid inclusion data. Eclogae Geologicae Helvetiae 73, 173–203.

Giorgetti, G., Memmi, I., Nieto, F., 1997. Microstructures of intergrown phyllosilicates grains from Verrucano metasediments (northern Apenines, Italy). Contributions to Mineralogy and Petrology 128, 127–138.

Giorgetti, G., Memmi, I., Peacor, D.R., 2000. Retarded illite crystallinity caused by stress-induced sub-grain boundaries in illite. Clay Minerals 35, 693–708.

Guidotti, C.V., Sassi, F.P., 1986. Classification and correlation of metamorphic facies series by means of muscovite b data from low-grade metapelites. Neues Jahrbuch für Mineralogie Abhandlungen 153, 363–380.

Guidotti, C.V., Yates, M.G., Dyar, M.D., Taylor, M.E., 1994. Petrogenetic implications of the Fe^{3+} content of muscovite in pelitic schists. American Mineralogist 79, 793–795.

Gutiérrez-Alonso, G., Nieto, F., 1996. White-mica "crystallinity", finite strain and cleavage development across a large Varisca structure, NW Spain. Journal of the Geological Society 153, 287–299.

Hibbard, J.P., Laughland, M.M., Kang, S.M., Karig, D., 1993. The thermal imprint of spreading ridge subduction on the upper structural levels of an accretionary prism. Southwest Japan. In: Underwood, M.B. (Ed.), Thermal Evolution of the Tertiary Shimanto Belt, Southwest Japan; An Example of Ridge–Trench Interaction. Special Paper - Geological Society of America, vol. 273, pp. 83–101.

Jiang, W.T., Lin, H.H., 2000. Mineralogy and low grade metamorphism of early paleozoic clastic rocks from eastern North Qilan fold belt. In: Yang, H.Y. (Ed.), Magmatism, Metamorphism and Structural Geology of the Qilian fold Belt, NW China. Journal of the Geological Society of China, vol. 43, pp. 15–30.

Johnson, M.R.W., Oliver, G.J.H., 1990. Precollision and postcollision thermal events in the Himalaya. Geology 18, 753–756.

Kanemoto, T., Otsuka, T., 2000. Illite crystallinity and low grade metamorphism of the Sanbagawa, Chichibu and Shimanto belts in the south area of Lake Suwa, central Japan. Journal of the Faculty of Science, Shinshu University 35, 11–29.

Khudoley, A.K., 1993. Structural and strain analyses of the middle part of the Talassian Alatau ridge (Middle Asia, Kyrgyzstan). Journal of Structural Geology 15 (6), 693–706.

Kisch, H.J., 1991. Illite crystallinity: recommendations on sample preparation, X-ray diffraction settings, and interlaboratory samples. Journal of Metamorphic Geology 9, 665–670.

Kiselev, V.V., Korolev, V.G., 1981. Paleotectonics of the Tien Shan Precambrian and Lower Paleozoic Ilim, Frunze. 60 pp. (in Russian).

Kiselev, V.V., Apayarov, F.H., Becker, A., 1988. The epibaicalic Precambrian of Tien Shan. In: Bakirov, A.V., Kiselev, V.V. (Eds.), The Precambrian and the Lower Paleozoic of Tien Shan. Ilim, Frunze, pp. 127–143 (in Russian).

Korolev, V.G., Maksumova, R.A., 1980. Flysch association of the upper Riphean of the Talas Range. International Geology Review 22 (3), 349–360.

Kretz, R., 1983. Symbols for rock-forming minerals. American Mineralogist 68, 277–279.

Kübler, B., 1968. Evaluation quantitative du métamorphisme par la cristallinité de l'illite. Bulletin du Centre de Recherches de Pau-SNPA 2, 385–397.

Li, G., Peacor, D.R., Merriman, R.J., Roberts, B., Van der Pluijm, B.A., 1994. TEM and AEM constraints on the origin and significance of chlorite–mica stacks in slates: an example from Central Wales, UK. Journal of Structural Geology 16, 1139–1157.

Maksumova, R.A., 1980. Baikalian orogenic complex of the Northern Tien Shan and Southern Kazakhstan. Ilim, Frunze. 150 pp. (in Russian).

Maruyama, S., Liou, J.G., Terabayashi, M., 1996. Blueschist and eclogites of the world and their exhumation. International Geology Review 38, 485–594.

Massone, H.J., Scherreyer, W., 1987. Phengite geobarometry based on the limiting assemblage with K-feldspar, phlogopite, and quartz. Contributions to Mineralogy and Petrology 96, 212–224.

Merriman, R.J., Frey, M., 1999. Patterns of very low-grade metamorphism in metapelitic rocks. In: Frey, M., Robinson, D. (Eds.), Low-Grade Metamorphism. Blackwell Science, Oxford, pp. 61–107.

Merriman, R.J., Peacor, D.R., 1999. Very low-grade metapelites: mineralogy, microfabrics and measuring reaction progress. In: Frey, M., Robinson, D. (Eds.), Low-Grade Metamorphism. Blackwell Science, Oxford, pp. 10–60.

Milodowsky, A.E., Zalasiewicz, J.A., 1991. The origin and sedimentary, diagenetic and metamorphic evolution of chlorite–mica stacks in Llandovery sediments of central Wales, UK. Geological Magazine 128, 263–278.

Offler, R., Miller, J. Mcl., Gray, D.R., Foster, D.A., Bale, R., 1998. Crystallinity and b_0 spacing of K-white micas in a paleozoic accretionary complex, eastern Australia; metamorphism, paleogeotherms, and structural style of an underplated sequence. Journal of Geology 106, 495–509.

Robinson, D., 1987. Transition from diagenesis to metamorphism in extensional and collision settings. Geology 15, 866–869.

Sassi, F.P., Scolari, A., 1974. The b_0 value of the potassic white micas as a barometric indicator in low-grade metamorphism of pelitic schists. Contributions to Mineralogy and Petrology 45, 143–152.

Sengör, A.M.C., Natal'in, B.A., 1996. Palaeotectonics of Asia: fragments and synthesis. In: Yin, A., Harrison, M. (Eds.), The Tectonic Evolution of Asia. Cambridge Univ. Press, Cambridge, pp. 486–640.

Sengör, A.M.C., Natal'in, B.A., Burtman, V.S., 1993. Evolution of the Altaid tectonic collage and Paleozoic crustal growth in Eurasia. Nature 364, 299–307.

Ujiie, K., 1997. Off-scraping accretionary process under the subduction of young oceanic crust; the Shimanto Belt of Okinawa island, Ryukyu Arc. Tectonics 16, 305–322.

Taylor, S.R., McLennan, S.M., 1985. The Continental Crust: Its Composition and Evolution. Blackwell, Oxford. 312 pp.

Warr, L.N., Rice, H.N., 1994. Interlaboratory standardization and calibration of clay mineral crystallinity and crystallite size data. Journal of Metamorphic Geology 12, 141–152.